1

CHAPTER 1: INTRODUCTION

1.1 BACKGROUND AND MOTIVATION

Energy is becoming an issue of serious concern in the world today. It is inevitable for human life and a secure supply of energy is required for sustainability of human societies [1]. The need to satisfy world energy demand, which actually determines the living standard of the populace, is increasing. This energy is utilised to generate the electricity we need for our homes, businesses, schools and factories. It energises our computers, lights, refrigerators, washing machines and air conditioners, to mention only a few. Also, the quantity of energy required in the industrial sector of the economy for its production activities is ever-increasing. This energy is mostly obtained from fossil fuel stock combustion processes and great deals of pollutant gases (CO_2, NO_X, etc.) are emitted to the atmosphere [2, 3]. Some of these gases, especially CO_2, are a major contributor to global warming and its attendant consequences, such as rise in global average temperatures, rise in sea levels, flooding and deforestation. Therefore, the effects of global warming have become an issue of major concern to goverments, policy makers and environmentalists. Hence, in recent times, numerous researches and commissioned studies have focused on the development of carbon-free energy sources that are environment-friendly, sustainable and cheaply available so as to minimise the amount of pollutant gases emitted into the atmosphere as a result of energy consumption [4].

The available energy sources in the world today are divided into two groups: renewable and non-renewable sources. Renewable energies are those that come from natural resources and are replenished naturally. Non-renewable energies are those that

are not replenished or only replenished very slowly. The available renewable energy systems range from solar power systems, wind power systems, geothermal power systems, fuel cells, etc. Renewable systems have different comparative advantages which usually determine their applications. Both renewable and non-renewable energy sources can be used to produce secondary energy sources, including electricity and hydrogen. However, most of our energy sources today are from non-renewable sources, which include the fossil fuels, i.e. oil, natural gas and coal [3]. Renewable energy resources become an important option to fossil fuel as the negative environmental consequences of fossil fuel increases and its utility cost (electricity) climbs. The quality of renewable energy technologies, that makes it a viable substitute to fossil fuel, includes its modular nature, lower operating cost and its flexibility and adaptability. These energy sources are considered by many as a direct replacement of existing fossil fuel technologies and this has made the evaluation of its benefit in terms of cost to be rated low when compared to traditional fossil technologies. The baseline is to view these renewable technologies as a complementary modular addition to existing energy systems with short lead-times [1]. This will adequately reduce the pressure on the national grids and ensure availability of energy to people in remote areas. Moreover, it will help reduce the amount of pollutant gases released into the atmosphere as a result of fossil fuel usage.

The world energy consumption projection by 2030 is estimated at about 700 Quadrillion British thermal unit (BTU) [5]. This figure equates to two-thirds more energy than the present usage. Fossil fuels will remain the dominant sources of energy, accounting for more than 90% of the projected increase in demand [5]. Problems associated with energy supply and demand are much more than global warming threats, but environmental concerns such as ozone layer depletion, pollution, deforestation and radioactive emission are increasing today [1]. These environmental problems need to be addressed quickly if the world is to achieve a sustainable energy future. The drive today is to seek for sustainable development through the utilisation of energy sources that has little or no adverse impact on the environment [6, 7]. These

energy sources (i.e. solar, wind, etc.) are easily replenished once consumed, as compared to finite fossil fuels (oil, coal and natural gas).

Hydrogen, a clean and renewable fuel source, is generally available in abundance and is a safe energy source [8, 9]. This fuel type can be generated from different kinds of sources, including most renewable sources and fossil fuels (natural gases and coal gasification). Figure 1.1 illustrates a typical comparison of utilising gasoline and hydrogen as fuel for transportation and mobile applications in the service sector [10]. The figure illustrates that hydrogen sources are diverse on the energy sector side and that the emission characteristics are quite limited on the service sector side, making hydrogen a key candidate for future energy currency.

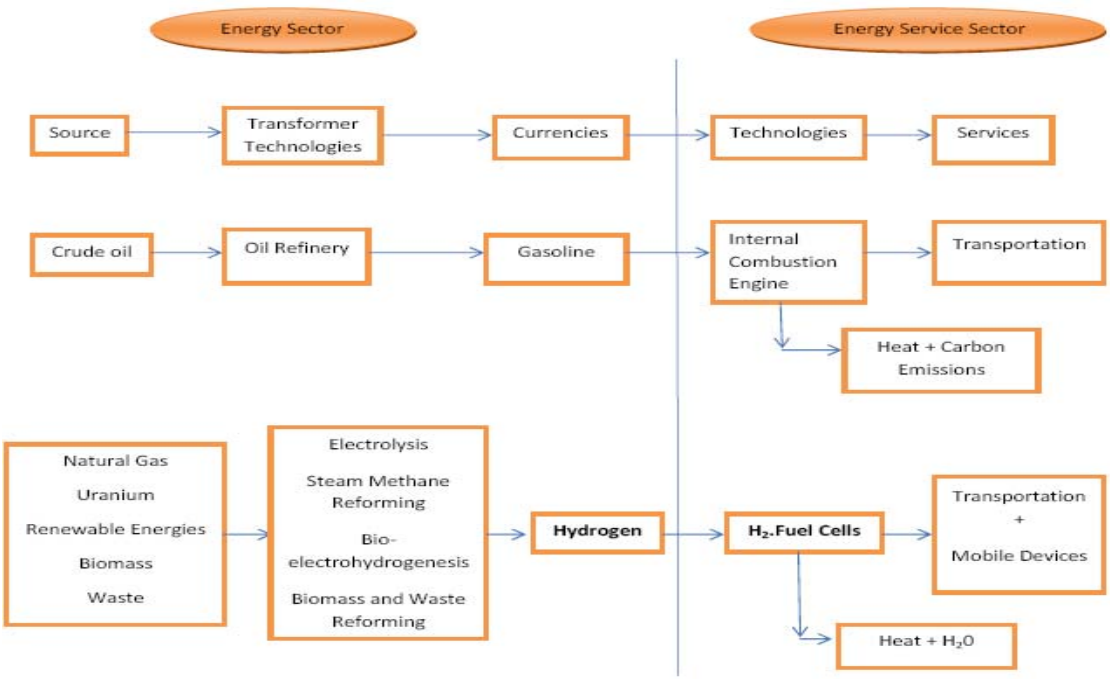

Figure 1.1 Comparison between hydrogen and gasoline as energy currency on service delivery chain [10]

Hydrogen has long been recognised as a potential fuel source for application in engines due to some unique and desirable properties [11]. These properties include its combustion in oxygen that produces only water as a waste, though, when combusted

in air, could generate some oxides of nitrogen. Table 1.1 is a comparison of combustion properties of hydrogen with other fuels. The table shows the outstanding properties of hydrogen in terms of performance when compared with other conventional fuels.

Recent studies [12-14] have shown the importance of hydrogen energy to sustainable development and in resolving the prevalent global environmental issues. The transition to hydrogen-based economy, where the main energy carrier is hydrogen and the main non-chemical energy form is electricity, is being made gradually and interest in this area is growing rapidly. However, generating electricity directly from hydrogen requires specific energy technologies such as the *fuel cell*. Fuel cell is a thermodynamic system that generates power by a direct conversion of the chemical energy in fuel into electrical power through electrochemical reaction [15].

Table 1.1 Combustion properties of hydrogen compared with other fuels [4]

Property	Hydrogen	Methane	Gasoline
Flammability limits (% by volume)	4-75	5.3-15.0	1.2-6.0
Minimum ignition energy (mJ)	0.02	0.28	0.25
Laminar flame speed at NTP (m/s)	1.90	0.38	0.37-0.43
Adiabatic temperature (°k)	2318	2190	~2470
Autoignition temperature (°k)	858	813	~500-750
Quenching gap at NTP (mm)	0.64	2.03	~2.0

Recent advancements in fuel cells have been driven by the demand for highly efficient power generation devices. Current fuel cell investments are mainly made by automotive industries to increase fuel efficiency and/or to use hydrogen as an alternative fuel. There are also opportunities of its application in power and electronic industries. The main reason for using fuel cells in power generation is the need for pollution reduction, back-up power, diversification of energy supply, as well as reduction in foreign energy dependency. Fuel cells are very useful as power sources in remote locations, such as spacecraft, remote weather stations, large parks, rural

locations and in certain military applications. A fuel cell running on hydrogen can be compact and lightweight, and have no major moving parts. A new application is micro combined heat and power (CHP), which is cogeneration for family homes, office buildings and factories [16].

Among the various types of fuel cells, *proton exchange membrane fuel cells* (PEMFCs), also termed "proton exchange membrane fuel cell" system, has attracted much interest as a convenient and viable alternative source of power, with promising potential to reduce the excess consumption of fossil fuel and discharge of carbon-dioxide [14]. The PEMFC has a high power density and a relatively low operating temperature (ranging from 60 to 80 degrees Celsius). The low operating temperature means that it does not take very long for the fuel cell to warm up and start generating electricity. Hence, PEMFC may most likely power automobiles and even residential houses in the nearest future.

Despite the potential of fuel cells to serve as clean alternative energy sources, a lot of issues still need to be addressed, mainly its cost of production and technical issues relating to optimal operating performance. The costs of components required to make fuel cells are prohibitive. For PEMFC systems, costly components such as proton exchange membranes, precious metal catalysts (usually platinum), gas diffusion layers and bipolar plates constitute up to 70% of the cost of a typical module [15]. Also, stationary fuel cell application typically require more than 40,000 hours of reliable operation at temperatures of -35°C to 40°C, while automotive fuel cells require a 5,000-hour lifespan (equivalent of 150,000 miles) under extreme temperatures. Automotive engines must also be able to start reliably at -30°C and have high power to volume ratio (typically 2.5 KW per liter). Thus, there is the need to develop fuel cells that are durable and can operate at temperatures greater than 100°C and yet function well at sub-zero ambient temperatures. In addition, the cell membranes also tend to degrade while the fuel cell system cycles on and off, particularly as operating temperatures rises. Hence, it is important for the membrane

to remain stable under cycling conditions. Also, PEMFC membranes must be hydrated in order to transfer hydrogen protons. This is necessary because, if water in the system evaporates too quickly, the membranes dry up and resistance across it increases. It will eventually crack, creating a gas "short circuit" where hydrogen and oxygen combine directly, generating heat that will damage the fuel cell. This condition necessitates that the fuel cell continues to operate in sub-zero temperatures, low humidity environments and high operating temperatures. Furthermore, when a fuel cell is in operation, the temperature must be maintained throughout the cell in order to prevent destruction of the cell through thermal loading. This is particularly challenging, since the reaction in the fuel cell is highly exothermic (heat releasing) and thus, large quantities of heat is generated within the fuel cell. Maintaining a uniform operating cell temperature in the fuel cell is thus not a trivial task.

The technical issues highlighted above, have hindered the commercialisation of PEMFC, hence there is need for in-depth research to understand and proffer solutions aimed at improving the performance of this class of fuel cell, so as to meet the market competitiveness compared to fossil-fuel based energy systems. One of the main objectives of the present fuel cell research in the industry today is the need to improve the performance of fuel cells. This can be done by better design and enhancing its capability so as to increase its production at low cost in order for it to compete favourably with fossil fuel-based systems. There are two primary approaches to achieving this, that is:

- Design, build and experimentally test approach to evaluate its performance

- Simulate by numerical modelling approach

The first approach usually yields useful and physical representative information of the phenomenon in the real system but is costly and time-consuming [10]. This becomes more difficult when looking into the vast number of working parts involved in a fuel

cell system and the limited experimental techniques available. The modelling approach can provide the much needed insight into the phenomena that characterise fuel cell systems at a reduced cost and time [10]. Optimal design of the system can thus be achieved and subsequently help at achieving the goal of fuel cell commercialisation. Performance improvement in the proton exchange membrane (PEM) fuel cell system is still an open research. More design models are being developed with the aim of enriching the knowledge base on generic information needed for a better design of PEM fuel cell systems. This research is one of the efforts channelled in that direction by introducing a more novel modelling approach coupled with optimisation techniques to improve the performance of PEM fuel cell systems.

1.2 REVIEW OF RELATED LITERATURE

A significant amount of research studies have been devoted to the study of PEM fuel cells, ranging from theoretical to experimental studies. With regards to the former, several empirical and mathematical models, which are aimed at understanding and predicting PEM fuel cell performance, have been proposed. Giner and Hunter [17] and Cutlip *et al.* [18, 19] have proposed the first of such models taking into consideration diffusion and reaction in the gas-diffusion electrodes. More attention subsequently spring up towards experimental studies [20-22] using simple 0-D models to analyse data on PEM fuel cells. These models normally fit the experimental data with a single equation. Although these models demonstrate good fits and are quick and easy to implement, they are less accurate and reliable in predicting the PEM fuel cell behaviour. More fundamental models were developed thereafter to simulate performance and gain deeper understanding of the underlying fundamental transport processes. Two main works in this regard are those of Bernadi and Verbrugge [23] (hereafter referred to as B&V) and Springer *et al.* [24]. Both studies included the membrane, diffusion media and catalyst layers in their respective models. B&V's model assumes a fully hydrated membrane and incorporates porous-electrode

equations and Stefan-Maxwell diffusion in the diffusion media and catalyst layers. The model of Springer *et al.* [24] does not use porous-electrode equations but changing water content in the membrane. This changing water content allows for variable properties in the membrane such as conductivity and the water diffusion coefficient. Most models today can conveniently trace their roots back to B&V studies [25].

The advances in digital computer technology have spurred the progress in the area of fuel cell development, especially in the application of numerical methods for fuel cell optimisation. The advancement in computational fluid dynamics (CFD) allows for effective design and optimisation of the fuel cell systems, with reduced reliance on hardware prototyping and reduction in development cycles. CFD provides a platform for understanding the variety of complex multi-physics transport processes characterised by a broad spectrum of length and time scales in the fuel cell structure. These processes include phenomena which involve fluidic, ionic, electronic and thermal transport in concert with electrochemical reactions. B&V's model forms the basis for almost all the CFD models in fuel cells today [25]. The incorporated electrochemical effects stem from the developed equations of B&V, such as their kinetic source terms in the catalyst layers and the use of Schlogl's equation for water transport in the membrane. The following sections (1.2.1-1.2.4) deal with specific literature relevant to this thesis, in which related studies addressing the design, optmisation and performance analysis of PEM fuel cells are discussed.

1.2.1 OPTIMAL OPERATING CONDITIONS FOR PEM FUEL CELL

Fuel cell operation involves the specification of a range of operating conditions such as temperature, pressure, stoichiometry ratio of reactant gases, porosity of the diffusion layers, etc. Accurate specification of this range of operating conditions will assist in predicting the fuel cell performance under these specified conditions and

could be used to optimise the design of a fuel cell system. Appropriate operating conditions are also required for a PEM fuel cell system to achieve and maintain stable operational performance. Effects of the gas hydrodynamics on the performance of the air cathode of a PEMFC with an interdigitated gas distributor has been studied by Yi and Nguyen [26]. In addition, pressure drop between the inlet and outlet channels, electrode height and shoulder width on the average current density were studied. They discovered that, with the forced flow-through condition created by the interdigitated gas distributor design, the diffusion layer thickness is greatly reduced. However, even with a much thinner diffusion layer, diffusion still plays a significant role in the transportation of oxygen to the reaction surface. In addition, the average current density generated at an air cathode increases with higher gas flowrates, thinner electrodes and narrower shoulder widths between the inlet and outlet channels of the interdigitated gas distributor.

Chan and Tun [27] conducted an investigation to determine the effects of the different parameters such as catalyst layer porosity, catalyst layer thickness and ionic conductivity on the performance of PEM fuel cells. The model showed that catalyst layer porosity and catalyst layer thickness has a significant effect on the limiting current density for the fuel cell. However, the ionic conductivity has no effect on the limiting current density. Furthermore, Jaouen *et al.* [28] used a one-dimensional, steady-state agglomerate model to determine the nature of mass transport limitations in the PEM fuel cell cathode. Effects of the active layer thickness, oxygen concentration and relative humidity of the oxygen stream were investigated. The result of the model shows that limitation by proton migration in the active layer, or by oxygen diffusion in the agglomerates leads to a doubling of the Tafel slope at higher current densities. For those two types of transport limitations, the dependence of the reaction rate on the active-layer thickness, oxygen partial pressure and relative humidity of the specie gas were shown. When additional limitation, due to slow gas phase diffusion, appears, the double Tafel slope is distorted. A mathematical

expression for the limiting current density, due to this process, was presented for use in correcting the polarisation curves for slow gas phase diffusion.

Studies on the effects of various operational parameters such as temperature, pressure, stoichiometric ratio, porosity and gas diffusion layer (GDL) thickness on the fuel cell performance was performed by Berning *et al.* [29]. They observed that temperature, pressure, stoichiometry ratio, GDL thickness and porosity, all have an impact on the limiting current density at a varying degree for the fuel cell. They also observed the need to estimate the extent of contact resistance inside the fuel cell in order to properly assess the impact of porosity and channel width on fuel cell performance. Kazim *et al.* [30] presented a two-dimensional mathematical model in which they investigated the effects of cathode porosity, inlet oxygen mole fraction, operating temperature and pressure on the performance of PEM fuel cells with the interdigitated flow field. The obtained result illustrated the positive impact of an increase in the GDL porosity on the fuel cell performance. Furthermore, it was observed that an increase in the mole fraction, operating pressure, or temperature of the oxygen entering the cathode GDL leads to higher fuel cell performance.

Chu *et al.* [31] studied the effect of variability in the porosity size of the GDL on the performance of PEM fuel cell. They observed that a fuel cell embedded in a GDL with a larger averaged porosity consumes a greater amount of oxygen, such that a higher current density is generated and a better fuel cell performance of the fuel cell is obtained. This explains partly why fuel cell performance deteriorates significantly as the cathode is flooded with water (i.e. to give a lower effective porosity in the GDL). In terms of the system performance, a change in GDL porosity has virtually no influence on the level of polarisation when the current density is medium or lower, but exerts a significant influence when the current density is high. The investigations of Jeng *et al.* [32] focused on the effects of the change in the porosity of the GDL on the performance characteristics of a PEMFC. Their results also showed that the existence of ribs causes the GDL to be used only partly in the mass transfer process.

The GDL's effectiveness decreases with the cell current density and increases with the width of the gas flow channels. The PEM fuel cell performance decreased with an increase in the GDL thickness when the GDL porosity is low. However, when a high-porosity GDL is used, the optimal thickness becomes an indicator which determines the maximal PEM fuel cell performance.

Wang *et al.* [33] conducted a study aimed at verifying the mechanisms of parameter effects and their interrelationship by comparing modelling results with experimental data. They observed that, when adequate humidification is provided, the performance of the PEM fuel cell improves with the increase in fuel cell temperature. The result also showed that anode and cathode humidification has significant effects on the performance of the PEM fuel cell. Lee *et al.* [34] conducted a numerical simulation of the species gas in the fuel channel and the diffusion layer to investigate the effects of GDL thickness, porosity and distribution of the pore size on the PEM fuel cell performance. The PEM electrodes were prepared by applying different porous GDLs onto each face of a carbon cloth support. They discovered that a GDL with a more porous structure performed better. More importantly, it was shown that a GDL's geometric characteristics (thickness, porosity and distribution of pore size) greatly affect the performance of the PEM fuel cell.

Hwang *et al.* [35] presented a three-dimensional numerical model to simulate the transport phenomena on the cathode air-side of a PEMFC. They compared the polarisation curves of the interdigitated flow field and parallel flow field for a typical PEM fuel cell. Their study ascertained the fact that an interdigitated flow field gives a higher average current density on the catalyst layer surface than with parallel flow field under similar mass flow rate and cathode overpotential. Effects of electron transport through the GDL of the PEM fuel cell was investigated by Meng and Wang [36]. They discovered that the lateral electronic resistance of the GDL, which is affected by the electronic conductivity, GDL thickness and gas channel width played a critical role in determining the current distribution and cell performance. It was further

observed that, under fully-humidified gas feed in the anode and cathode, both oxygen and lateral electron transport in the GDL dictated the current distribution. The lateral electronic resistance dominated the current distribution at high cell voltages, while the oxygen concentration played a more decisive role at low cell voltages. With reduced GDL thickness, the effect of the lateral electronic resistance on the current distribution and cell performance became even stronger, because the cross-sectional area of the GDL for lateral electron transport was smaller.

Du *et al.* [37] proposed a theoretical model to investigate the effective protonic and electronic conductivity of the catalyst layers in PEM fuel cells. The model showed that effective protonic conductivity increased with an increase in the Nafion volume fraction in the catalyst layers of the PEM fuel cells. The study also showed that effective protonic conductivity increased almost linearly with an increase in the operating temperature for a given water activity. Pasaogullari and Wang [38] conducted an investigation on the two-phase flow characteristics in the cathode GDL of a PEMFC. They revealed that an onset of flooding of the porous cathode hinders the rate of oxygen mass transport to the cathode catalyst layer. In addition, their result showed that the rate of cell humidification and mass flow rate of the reactant gas species are important parameters determining PEMFC two-phase flow transport characteristics and performance.

Lu and McGurick [39] presented a model of the PEMFC cathode with an interdigitated gas distributor to investigate the effects of various parameters such as electrode permeability, thickness and shoulder width on the cell performance. It was observed that changes in permeability, ranging from 10^{-8} to 10^{-13} m^2, has little impact on the cell performance. Increasing the electrode thickness and the shoulder width resulted in poorer performance due to greater resistance to flow. In addition, their results showed that liquid water tends to form near the outlet of the electrode when the current density is greater than 1.0×10^4 A m^{-2}. Sun *et al.* [40] developed a two-dimensional model to investigate the influence of the GDL property and flow-field

geometry, such as diffusion layer diffusivity, diffusion layer conductivity, channel width-to-area ratio and diffusion layer thickness on the local reaction rate in the PEMFC cathode catalyst layer. Their work showed that, when the PEMFC is operated using reformate hydrogen, the performance drops dramatically due to carbon monoxide (CO) poisoning as the anode gas flow rate increases. More research on the CO poisoning effect on PEMFC performance are reported in the literature [41-43].

Mawardi and Pitchumani [44] studied the effect of parameter uncertainty on the variability in performance of PEM fuel cells and optimisation of different operating parameters that affects fuel cell performance. They developed a sampling-based stochastic model to measure the performance of PEM fuel cells. The results further provided a valuable tool for the design of fuel cells under uncertainty in material and operating parameters.

Hsieh *et al.* [45] investigated the effects of the operating temperature and backpressure on the performance of micro PEM fuel cells using different flow fields. Their study concluded that cell performance increases with an increase in cell operating temperature until a limiting or threshold level is reached. In addition, they observed that the higher the flow-back pressure, the better the performance of the single micro PEMFC at a fixed cell operating temperature. The interdigitated flow field showed better performance, while lower pressure was obtained using mesh-type flow field at a fixed active area of the membrane electrode assembly (MEA).

Yan *et al.* [46] investigated the steady and transient response on performance in both single fuel cell and stack configuration under a variety of loading cycles and operating conditions. They discovered that different feed gas humidity, operating temperature, feed gas stoichiometry, air pressure, fuel cell size and gas flow pattern affect both the steady-state and dynamic response of fuel cells. They experimentally confirmed that a decrease in the cathode humidity has a detrimental effect on the fuel cell steady state and dynamic performance of the fuel cell. Temperature variation also significantly

affects fuel cell performance through its effect on membrane conductivity and water transport in the GDL and the catalyst layer. Amirinejad *et al.* [47] conducted experiments to study the effects of operating parameters on PEM fuel cell performance by using dry and humidified hydrogen and oxygen as reactant and oxidant gases, respectively. The result of their experiment showed that the most important factor affecting the PEMFC performance is the mass transport limitation. This limitation included the transport of reactant and oxidant gases to active sites of the catalyst, the transport of the proton from the anode side to the cathode side through the membrane, and the transport of produced water from the cathode side to the anode side by back-diffusion mechanism. Fuel cell operating parameters such as temperature, pressures and humidity of reactant gases could decrease the mass transport limitation and improve the performance of the fuel cell.

Zhou *et al.* [48] developed a steady-state, two-dimensional model to illustrate the inlet humidification and pressure effects on PEM fuel cell performance. Their model asserts the fact that humidification of both the anode and the cathode is very important for fuel cell performance. Also, the pressure drop in the PEM fuel cell flow channels increases the pumping power requirement and attention must be paid to this pressure situation when designing the fuel cell. Yan *et al.* [49] determined the electrical characteristics of a PEMFC stack under varying operating conditions, using AC impedance measurement technique. They documented the fact that the air humidity and cell temperature greatly impact on the charge transfer resistance of the PEM fuel cell stack. Similar to Yan *et al.*'s work is studies by Zhang *et al.* [50]. They investigated the effect of reactant gas relative humidity on fuel cell performance using the AC impedance and cyclic voltammetry methods. This study affirmed that a reduction in the relative humidity of a fuel cell can depress the electrode kinetics, including electron reaction and mass diffusion rates, and the proton conductivity of the membrane, resulting in a dramatic degradation of the fuel cell performance.

Hung *et al.* [51] developed a theoretical model to investigate the effects of operating parameters (e.g. temperature, humidification temperature, pressure, gas stoichiometry ratios) on cell performance. Design and modelling parameters were obtained using a regression analysis of experimental data and validating it as these operating parameters changes. Hwang *et al.* [52] presented a non-isothermal model of PEMFC in contact with an interdigitated flow field to study the effect of flow orientation on thermal-electrochemical transport in a PEM fuel cell. The study revealed that both the solid-matrix and fluid-phase temperatures are increased with the increase of the total overpotential of the fuel cell. In addition, the fluid-phase and solid-matrix temperature distributions are significantly affected by the flow orientation of the species reactant in the PEM fuel cell.

Yuan *et al.* [53] proposed a three-dimensional multi-phased model of a PEM fuel cell to predict the effects of operating parameters on the performance of PEM fuel cells. The study revealed that fuel cell performance is enhanced with an increase in operating pressure, temperature and air stoichiometry ratio. The study asserts the fact that anode humidification has more significant effects on the PEM fuel cell performance than cathode humidification. It was also documented that best performance occurred at low air relative humidity and high hydrogen relative humidity.

In summary, most theoretical studies on fuel cells in the literature focus on the numerical simulation of the transport phenomenon and parametric study of the effects of physical variables. The main objectives of the reported models are to investigate the performance of fuel cells under various operating conditions, with a view to find optimal performance parameters.

1.2.2 FUEL GAS CHANNEL OPTIMISATION FOR PEM FUEL CELLS

One of the critical issues in proton exchange membrane fuel cell design is the efficient design of the flow channels to ensure uniform distribution of the reactant gases in the fuel cell stack. The flow field geometry and pattern has great influence on the reactant gas transport, water management and the efficient utilisation of the fuel gases, since efficient species gas transport and water removal from the fuel cell system is enabled by proper flow field design. The flow field design for fuel cells is thus one of the important technical challenges for PEM fuel cell design and operation and impacts on system performance and life-span [54].

Kumar and Reddy [55] studied the effect of the dimensions and shape of the flow channels in the flow-field of a PEMFC. The flow field used for the study was the single-path serpentine design. They concluded from their study that optimum channel width, land width and channel depth for optimal fuel cell performance are close to values of 1.5, 0.5 and 1.5 mm, respectively. In addition, it was found that reducing the channel land width, increases the hydrogen consumption at the anode section of the fuel cell. A hydrodynamic model to study flow distribution and pressure drop in parallel-channel configurations of a planar fuel cell was developed by Maharudrayya *et al.* [56]. They considered Z-type and U-type configuration channels in their study. The obtained result shows that for a fuel cell distributor plate, low and high flow maldistribution could occur for both the Z-type and U-type configuration. The extent of this maldistribution is a function of the geometric factors of the parallel-channel configuration and these factors could be manipulated to achieve a uniform flow distribution in the fuel cell system.

Shimpalee *et al.* [57] investigated the impact of channel path length on a PEMFC system. They concluded from their work that better uniformity in local temperature, water content and current density distribution in the serpentine flow-field design of the PEM fuel cell system is obtained by using a shorter path length rather than a

longer path. Hence, reducing the PEM flow-field path length is a prospective variable for improving the performance and efficiency of the PEMFC system. Inoue *et al.* [58] conducted a study to investigate the effect of gas channel depth on current density distribution of PEM fuel cell using computational fluid dynamics, including gas flow through a GDL. They found that output current density of the fuel cell system increases with the decrease in the depth of the separator channel and corresponding increase in pressure drop and current density distribution.

A model similar to that of Inoue [58], was employed by Ahmed and Sung [59] to investigate the effect of channel geometric configuration at high operating current density of the fuel cell. Their result demonstrated the fact that a rectangular channel cross-section produces higher cell voltages compared with trapezoidal and parallelogram channel cross-sections. However, the trapezoidal cross-section proves more effective at ensuring uniform reactant and local current density distribution over the reactant area of the fuel cell. The results further ascertain the fact that shoulder width impacts great on fuel cell performance when compared with other geometric factors. Also, Cheng *et al.* [60] conducted a study to optimise the geometrical parameters of the PEMFC, by using a numerical approach coupled with an optimiser. The result of their study shows that the gas channel width fraction, the gas channel height and the thickness of the GDL all influenced the performance of the fuel cell system. In addition, their study shows that, using the coupled optimiser at channel width fraction of 0.3925, gas channel height of 1.2034 mm and GDL thickness of 0.176 mm, an optimal power density of 1857 W m^{-2} is obtained when compared with the original fuel cell design.

Xu and Zhao [61] developed a novel flow-field for polymer electrolyte-based fuel cell systems by re-pattering conventional single serpentine flow fields. Their studies confirmed the effectiveness of this new design at inducing larger pressure difference between adjacent flow channels over the electrode surface area of the fuel cell. The effect of such large difference is that mass transport of the reactant gases and products

are enhanced to and from the catalyst layer. Furthermore, water clogging within the electrode in greatly reduced.

Li *et al.* [62] proposed a flow-field design procedure to effectively eliminate resident water flooding in the PEM fuel cells. They employed a design based on specifying appropriate pressure drop along the flow channel that will ensure evaporation or drift force removal by the gas stream in the flow channel width, therefore, dehydrating the fuel cell membrane. They reported that the designed flow-field procedure is effective for water removal in the fuel cell. Their claims were validated experimentally, by using a neutron imaging technique measurement of liquid water content in the fuel cell system. Shimpalee and van Zee [63] numerically investigated the effect of rib and channel dimension of the reactant flow-field on the performance of PEMFC under automotive and stationary conditions. The obtained result revealed that, for stationary applications, employing a narrower channel with widened rib spacing produces higher fuel cell performance, with the reverse being a case of automotive application.

Owejan *et al.* [64] studied the effects of flow field and GDL properties on water accumulation in the PEMFC. They documented that flow field channels with hydrophobic coating retain more water in the fuel system, but the spread of a higher number of smaller water slugs improves the fuel cell performance at high current density. The result further demonstrated the fact that cells made by using diffusion media with lower in-plane gas permeability shows lower water accumulation capacity in the fuel cell system. Peng *et al.* [65] developed a model to optimise the flow channel design and at the same time balance the fuel cell stack performance and formability. Their optimisation result shows that optimum dimensional values for channel depth, channel width, rib width and transitional radius of 0.5, 1.0, 1.6 and 0.5 mm, respectively, were obtained at highest reaction efficiency of 79% and formability of 1.0 of the fuel cell used for their study.

Sinha *et al.* [66] presented a three-dimensional, non-isothermal PEMFC model to investigate the effect of flow field design on the performance of the system at elevated temperatures. They compared the fuel cell performance with serpentine and parallel flow field design when the fuel cell is operated at 95ºC under various inlet humidity conditions. They concluded that the parallel flow field design ensure better and uniform distributed performance on the entire cell active area when compared to the serpentine flow field at low inlet relative humidity and elevated temperatures. Hsieh and Chu [67] conducted a study on channel and rib geometric scale effects of flow-field plates on the performance and transient thermal characteristics of micro-PEM fuel cell system. They found that optimum channel-to-rib width ratio for the range considered in their study to be 0.67, considering the net power gain of the system. In addition, they documented the fact that channel and rib geometric effect has no significant effect on the cell system transient temperature distribution.

Ferng *et al.* [68] performed a numerical and experimental investigation into the effects of flow channel patterns on the performance of PEM fuel cell by using parallel and serpentine flow channels with the single path of uniform depth and four paths of step-wise depth, respectively. They documented in their study that the serpentine flow channel is better when compared with the parallel flow channel. Their result further shows that different depth of the flow channel significantly affect the performance of the parallel design but have no significant effect on the serpentine channel design performance. Wang *et al.* [69] studied the local transport phenomena and PEM fuel cell performance with various serpentine flow field designs. The study considered single, double and triple serpentine flow field designs. The predicted results was confirmed, i.e. that the single serpentine flow field has better performance when compared with double and triple serpentine designs and the performance of the single serpentine flow field increases as the number of the channel bend is increased. It was also found that the performance of the fuel cell increases slowly as fuel channel width increases.

Finally, a comprehensive review on flow field design in the bipolar plates of PEM fuel cells has been published by Li and Sabir [70]. They presented reviews on various flow-field layouts developed by different companies and research groups. Furthermore, they enumerated and evaluated the pros and cons in those various designs. In addition, the review concluded that improvement on flow-field design for fuel cells can greatly improve the goal of cost reduction and performance enhancement for the commercialisation of PEM fuel cell. However, flow-field design is still an open ended on-going research and more novel designs, that will be suitable for different and specific applications, are required.

1.2.3 REACTANT GAS TRANSPORT IN PEM FUEL CELLS

Flow distribution in PEMFC impacts greatly on the performance and efficiency of the system. The efficient distribution of species reactant to ensure homogenous spread on the GDL at reasonable pressure drop along the flow channel distributor is crucial to both effective utilisation of fuel gases and PEMFC performance. In addition, proper water and heat management within the fuel cell structures are required for obtaining optimal power density from the fuel cell. Hence, enormous efforts are being devoted by various researchers to develop novel flow structures for PEM fuel that will enhance the interaction between the GDL and the flow field to improve the cell performance. A discussion on these research efforts follows.

Um *et al.* [71] developed a transient, multidimensional model to investigate the electrochemical and transport processes inside a PEMFC. They reported that, in the presence of hydrogen dilution in the PEM fuel stream, there is a large decrease in hydrogen presence at the reaction surface which results in lower current density as a consequence of decreased hydrogen transport to the reaction site of the fuel cell system. He *et al.* [72] presented a two-phase model of the cathode of the PEMFC by using interdigitated flow fields. The model was used to investigate the effect of

various electrode and flow field design parameters at the cathode of PEM fuel cell performance. Their result shows that liquid water transport and evaporation form the mechanism for water removal at the cathode section of the PEM fuel cell. Also, higher differential pressure between inlet and outlet channels increase oxygen transport and liquid water removal from the electrode section, thereby increasing the fuel cell performance. They further suggested the need to optimise the electrode thickness for better PEM fuel cell performance.

Chang *et al*. [73] studied flow distribution in the PEM fuel cell stack system, incorporating flow diffusion effects into their model. They reported that higher channel friction factors leads to more uniform flow distribution in the fuel system and the U-type manifold design performs better than the Z-type design. In addition, they observed that, at higher current densities, fuel cell performance is more sensitive to operating conditions such as cathode stoichiometry and inlet pressure. Mazumder and Cole [74] studied liquid water transport in PEM fuel cells using a three-dimensional model. They concluded that, at critical current density, saturation levels could exceed 50% and are more prominently so at the cathode section of the fuel cell. In addition, they also reported that the effect of electro-osmotic drag contributes majorly to the determination of the local saturation level in the MEA of the fuel cell, but was found negligible at impacting on the fuel cell performance.

Dohle *et al.* [75] proposed a model to evaluate the interaction between the GDL and the flow field of PEMFC. Their model was also utilised to develop a suitable match between serpentine flow field and the diffusion layer of the fuel cell system. They reported that, to avoid reactant depletion in the specific region of the fuel cell, the geometry of the serpentine channel should be chosen with regard to permeability of the GDL. In addition, to obtain higher permeability, the serpentine structure should have low pressure loss to ensure good flow homogeneity. In the studies of Gurau *et al.* [76], a multifluid, multiphase model was proposed to evaluate the two-phase transport in PEMFC. The model developed accounts for gas- and liquid-phase

momentum and species transport in the whole structure of the PEM fuel cell system. They documented that the level of water accumulation in the GDL is predominantly determined by the saturation equilibrium at the GDL-channel interface and the GDL permeability. Meanwhile, the level of water accumulation in the catalyst layer is determined by the saturation level in the GDL and the saturation equilibrium at the GDL/catalyst layer interface.

Yan *et al.* [77] presented a model to investigate the effect of flow distributor geometry and diffusion layer porosity on reactant gas transport and PEM fuel cell performance. They reported that increase in channel width fraction, number of channels and porosity of the GDL positively enhance the performance of the studied fuel cell system. In addition, the results shows that better uniformity in current density along the width of the cell can be obtained at relatively low overpotential of the fuel cell. Wang *et al.* [78] proposed a novel serpentine-baffle flow field design, different from conventional serpentine flow field, to improve the PEM fuel cell performance. The model developed was also used to analyse the reactant and product transport and the electrochemical reactions in the fuel cell. They concluded that, at high operating fuel cell voltages, conventional and baffled novel serpentine design shows the same performance. However, at lower operating cell voltages, the baffle design shows better performance than the conventional design. Their result further shows that larger pressure differences are induced on the electrode surface with baffled channels. Consequently, the mass transport is improved, thereby leading to enhanced fuel cell performance.

Jang *et al.* [79] developed a two-dimensional model to investigate the performance of a PEM fuel cell system based on variability in porosity and GDL thickness. Their result shows that the mass transfer increment resulting in high reaction rates can be achieved by increasing the GDL porosity. This improves the fuel cell performance. In addition, they documented that the performance of the fuel cell also increases with the decrease in the thickness of the GDL. However, performance is enhanced in the fuel

cell system by using a co-flow of fuel and air rather than counterflow configuration. Wang *et al.* [80] presented a three-dimensional model of PEM fuel cells with parallel and interdigitated flow fields to investigate the effects of the cathode flow rate and flow channel area ratio on the cell performance. The model also incorporated the effects of liquid water formation on the reactant gas transport in the fuel cell system. It was documented that the performance of the fuel cell system is not impacted at high operating voltages by flow channel designs and operating parameters, but these parameters have a significant effect on the fuel cell performance at low operating voltages. Their result further shows higher performance of the fuel cell system when using interdigitated flow fields, owing to the forced convection created by its baffles to improve transport rates and liquid water removal.

Kim [81] investigated the effect of relative humidity and stoichiometry of reactants on water saturation and local transport process PEMFCs. The result shows that the reactant relative humidity (*RH*) and stoichiometry significantly affect the fuel cell performance. Also, at a constant relative humidity of the anode, *RH* = 100%, a lower cathode relative humidity maintains membrane hydration, resulting in improved fuel cell performance. Conversely, at a constant cathode *RH* of 100%, a lower anode *RH* increases the difference in water concentration between the anode and cathode, resulting in better fuel cell performance. In addition, higher anodic stoichiometry results in the reduction of cathode water saturation due to increase in back-diffusion, thereby increasing the fuel cell performance. Jang *et al.* [82] investigated the effect of humidity of reactant fuel on the cell performance of PEMFC with baffle-blocked flow field designs. They reported that fuel cell performance is enhanced with an increase in inlet *RH* of the hydrogen gas species due to an increase in the chemical reaction and mass transfer of oxygen. There is an adverse effect in performance by increasing the inlet *RH* in the cathode at lower cell voltage due to oxygen depletion in the fuel cell. Their result further shows that cell performance is enhanced with an increase in the number of baffles as a result of an increase in areas of forced convection and oxygen gas diffusion to the catalyst layer. Furthermore, Nguyen and White [83] developed a

model to investigate the effectiveness of varying humidification designs in PEM fuel cells. The model accounts for electro-osmotic and diffusion of water transport in the membrane, a solid phase to gas phase heat transfer and latent heat formation, resulting from evaporation and condensation in the flow channels. Their results show that, at high current densities, large fraction of voltage losses in the cell is due to ohmic loss in the membrane. They proposed that the anode gas stream must be humidified in order to maintain adequate hydration in the cell, especially when the fuel cell is operated at high power densities.

Ko *et al.* [84] investigated the effect of the channel flow pattern on internal properties distribution of a PEM fuel cell for cathode starvation conditions, numerically and experimentally. The fuel cell system performance was investigated by using single, double and mixed serpentine fuel channel configurations. They documented that mixed serpentine channels enhance flow velocity better than other configurations (single and double) and subsequently prevent the channel from flooding. Their result further shows that local temperature and sensitivity to cathode starvation is higher in single serpentine systems than in other configurations and that it is more liable to thermal degradation. Liu *et al.* [85] investigated the application of baffle-blocked flow channel for enhancement of reactant transport and performance of fuel cells. Their result shows that local transport of the reactant gases, current density output and cell performance can be enhanced by the incorporated baffles in the fuel cell flow channel. They further documented that baffle effects enhance gas fuel transport at high operating cell voltages and raise the local current density in the upstream, but lower them at the downstream of the channel.

Soong *et al.* [86] proposed a novel configuration of partially blocked fuel channels with baffle plates transversely inserted in the channel. They evaluated the effects of the blockage with various gap ratios, number of baffle plates, fuel flow Reynolds number and GDL porosity on reactant gas transport and pressure drop across the channel length. They documented that, reducing the gap size between the baffle and

the GDL and/or increasing the baffle number enhances the reactant gas transport but with adverse penalty of high pressure drop. They further proposed that, to ensure high performance and minimal pressure drop, a baffle gap ratio no smaller than 0.1, baffle plates number between 3 to 5 and GDL porosity of about 0.7 will be preferable as design values. Liu *et al.* [87] proposed a model to investigate the reactant gas transport and the PEM fuel cell performance with a tapered flow channel design. Their result shows that fuel cell performance is enhanced by using the tapered flow field design but more prominently so at lower cell voltages. They further documented that the liquid water effect has significant impact on transport phenomena and the performance of PEM fuel cell.

1.2.4 HEAT TRANSPORT AND COOLING IN PEM FUEL CELLS

Thermal management in PEM fuel cells has drawn increasing attention in recent times because technological limitations encountered in PEM fuel cells today depend largely on these aspects [88]. Operating temperature affects the maximum theoretical voltage at which a fuel cell can operate. Higher temperatures correspond to lower theoretical maximum voltages and lower theoretical efficiency [89]. However, increase in temperature at the electrodes increases the electrochemical activity, thereby increasing the fuel cell efficiency. Higher temperature operation of the fuel cell also improves the quality of waste heat derivable from the system. Practically, there is an optimal temperature range within which a specific fuel cell system can perform well and reliably. The main purpose of thermal management in fuel cell systems is to ensure effective stack operation within the specific temperature range. In recent years, efforts have been made to investigate and predict heat/mass transfer phenomenon in PEM fuel cell systems. Some of these research efforts are highlighted below.

Coppo *et al.* [90] presented a 3-D model to study the influence of temperature on the PEM fuel cell operation, including two-phase flow in the gas distribution channel.

The result obtained indicate that both liquid water transport within the GDL and liquid water removal from the surface of the GDL play an important role in determining variations in cell performance where temperature is involved. Yan *et al.* [91] presented a 1-D non-isothermal model to analyse the effect of anode and cathode side temperatures on the membrane water distribution. The results obtained shows that increasing the temperature on the anode side can lead to membrane dehydration, and operating the fuel cell at high current density leads to membrane dehydration on the anode side, due to strong electro-osmotic water drag at high current density.

Ramousse *et al.* [92] developed a 1-D non-isothermal model accounting for heat and mass transfer in a complete cell, and charge and mass transfer in the electrodes. Their study provides for temperature, concentration and potential fields in a single cell. In addition, their work shows that the thermal gradient in MEA could lead to thermal stresses at high current densities. Shimpalee and Dutta [93] conducted a 3-D non-isothermal numerical analysis with a two-phase flow. The effect of heat produced by the electrochemical reaction and phase change of water on the cell performance was critically studied. Their study shows that inclusion of heat transfer in the fuel cell model shows degradation in the fuel cell performance. This research work enumerated the importance of incorporating the heat transfer aspect in fuel cell modelling.

Shan and Choe [94] presented a 1-D model, taking into account the dynamics in temperature gradient across the fuel cell; dynamics in water concentration redistribution in the membrane; dynamics in proton concentration in the cathode catalyst layer; and dynamics in reactant concentration redistribution in the cathode GDL. Their result generally shows that temperature profiles in each of the cell layers tend to follow the current waveform, due to energy losses in these layers. Higher temperature losses are prominent in the membrane and the catalyst layer, due to ohmic losses as a result of membrane resistance and heat released by the chemical reaction. Yuan and Sunden [95] performed a 3-D non-isothermal numerical analysis of heat transfer and gas flow in PEM fuel cell ducts by using a generalised extended

Darcy model. Effects of the effective thermal conductivity, permeability, inertia coefficient and porous layer thickness on gas flow and heat transfer were studied. Their result shows that higher permeability, higher effective thermal conductivity of porous GDL and smaller thickness of the porous layer improved heat transfer in the modelled fuel cell system.

Ju *et al.* [96] presented a 3-D non-isothermal, single-phase model for all seven layers of the PEM fuel cell that accounts for various location-specific heat-generation mechanisms, including irreversible heating due to electrochemical reactions, heating due to entropy, and Joule (ohmic) heating due to membrane ionic resistance. They observed that the thermal effect on PEM fuel cells becomes more critical at higher cell current density and/or lower GDL thermal conductivity. Their result further shows that temperature increase in the membrane is highly dependent on the GDL thermal conductivity and inlet humidity conditions. Perng and Wu [97] proposed a semi-implicit finite element model to investigate the blockage effect generated by a baffle plate or a rectangular cylinder and its effect on the heat transfer enhancement in a PEM fuel cell with the catalyst layer kept at a constant heat flux. Their results show that the installation of transversely placed baffle plates and a rectangular cylinder in the flow channel effectively enhance the local heat transfer performance of the fuel cell system. Meanwhile, the rectangular cylinder has better effective heat transfer performance than a baffle plate, and the larger the cylinder width, the better the heat transfer performance becomes.

Yu *et al.* [98] presented a two-phase model with phase change to investigate the liquid water effect, especially how the inlet water (liquid or vapour) effects on the Ballard PEM fuel cell performance. The results of their study shows that, for the studied Ballard PEM fuel cell stack, the more the water supplied to the anode from its inlet, the higher the voltage and usually the lower the anode exit temperature. Berning and Djilali [99] developed a 3-D model to account for heat and mass transfer in a multicomponent two-phase flow, considering all seven layers of a PEM fuel cell and

the cooling channels. The results of their study show that phase change occurs at both sides of the fuel cell and these phase changes are due to an intricate balance of three competing processes: temperature change, reactant gas depletion and pressure drop inside the GDL. In addition, their study shows that the amount of liquid water formed depends largely on the GDL permeability. Also, condensation as well as evaporation takes place at the cathode GDL, whereas only condensation occurs at the anode GDL except near the inlet.

Kang *et al.* [100] investigated the effect of the inlet temperature and flow configuration on the species, hydration and temperature distribution in a PEM fuel cell system using the quasi-three-dimensional model. The results show that, of all the configurations studied, the configuration that has a fuel-air counter flow and an air-coolant co-flow, has the highest performance in all the ranges of current density because the membrane remains the most hydrated. In addition, they observed that, when the operating current density increases, the effect of temperature on membrane hydration slightly decreases. They concluded that it is possible to lower the fuel cell operating temperature to improve the fuel cell hydration which, in turn, improves fuel cell performance. Also, different flow configurations were observed to have effect on the pressure losses and local current density, membrane hydration and species mole fraction in the studied fuel cell system.

1.3 JUSTIFICATION FOR THIS STUDY

The need for commercialisation and economically viable PEMFCs necessitates further in-depth research into fuel cell designs. Although, there is extensive literature on methods and techniques that are aimed at optimising PEM fuel cell performance, critical issues remain in understanding how different parameters and modifications of the internal structures relates to affect the performance of the fuel cell under real operating conditions. Fuel cell structures such as the gas channels, reactant species

distribution and thermal conditioning greatly impact on the performance of the fuel cell system. Consequently, they are the subject of extensive theoretical and experimental investigations. In the research studies reported in this thesis, the focus is on the numerical approach to fuel cell engineering design, with specific exploration of a unique combination of computational fluid dynamics (CFD) and a robust mathematical optimisation tool to gain deeper understanding of how different fuel cell design parameters interact to determine the overall fuel cell performance. Furthermore, this study identifies novel optimisation techniques that, if integrated into development procedure, will enhance PEM fuel cell performance. The numerical approach implemented in this work provides an exceptional optimisation approach that can be used in determining a combination of optimum operating parameters for fuel cells under real-life operating conditions. In addition, our approach ensures minimum errors in optimised fuel cell design parameters.

Numerical modelling in recent times has made the development of CFD codes more robust. The availability of CFD codes has made it possible to perform an analysis on a series of parametric design variants until a satisfactory design criterion is obtained, whereafter a prototype development can take place. This will greatly reduce the lead time and cost in actual development procedures. Further improvement in the system design process is the use of mathematical optimisation tools. These optimisation tools can be used to overcome the problems of obtaining optimum design which was previously largely constrained by the skill and experience of the modeler. The combination of the computational fluid dynamics and mathematical optimisation can produce great improvement in the design process. This will ultimately reduce the lead time, cost and ease of obtaining generic information needed for better and efficient design of the fuel cell system. This work seeks to develop innovative approach, through modeling and optimisation, aimed at further enhancing PEM fuel cell performance within the identified limiting factors such as: ***operating conditions, channel geometry, reactant gas transport and thermal cooling approach,*** which are very crucial to fuel cell operation.

1.4 RESEARCH OBJECTIVES

The main aim of this research is to investigate on new approaches towards performance enhancement in PEM fuel cell system through numerical modelling and optimisation. It is anticipated that this would provide new insights into new approaches for PEM fuel cell system design technology. It is hoped that this information will be useful in maximising the efficiency and attainment of the commercialisation drive on this new energy technology. In order to realise the aim mentioned above, this study will focus on the following specific research activities:

- to numerically predict the performance of PEMFCs under different operating conditions by using a CFD code;

- to optimise the performance of PEMFCs through gas channel modification, taking into consideration the mass flow rate and porosity nature of the GDL;

- to develop a novel design approach that can improve the reactant species distribution on the GDL, hence improving the performance and reducing parasitic pump power losses;

- to investigate numerically cooling channel geometry scheme in conjunction with operating parameters (that are temperature-related) of PEM fuel cell systems that will allow operation of low temperature PEM fuel cell beyond the critical temperature ($\leq$ 80ºC) to intermediate high temperatures (100-150ºC), without the need for special compatible high temperature resistant materials which are relatively costly.

- to carry out the numerical model validations on the investigated fuel cell models.

The study emphasises that the attainment of these objectives will provide comprehensive understanding of how different fuel cell design parameters interact to improve the performance of PEM fuel cell systems. Some manufacturing parameters and novel approaches are established to optimise the performance of fuel cell systems. In summary, results from this study will lead to improved performance and design information needed for fuel cell manufacturers, which can be applied for better designs of fuel cell stacks.

1.5 ORGANISATION OF THE THESIS

The thesis is presented in a multiple manuscript format for better organisation and ease of reading. Chapters 4, 5, 6 are written as individual research papers. The thesis consists of the following chapters:

- **Chapter 2** gives an in-depth view into relevant literature related to the fundamental structures of a PEMFC and discusses the function of these features in relation to system performance. This chapter also presents the basic transport and electrochemical processes in PEMFC systems.

- **Chapter 3** exhibits an appropriate framework pertaining to the numerical modelling of PEMFC used in this study. Furthermore, the Dynamic-Q algorithm, used for the mathematical optimisation part of this study, is discussed in detail.

- **Chapter 4** deals with the numerical study on the effect of key operating parameters that impact on the performance of PEM fuel cells. The parameters investigated are both design and physical parameters. In addition, numerical optimisation of the fuel cell gas channel is carried out with interest on mutual interdependence of the GDL porous medium, reactant gas flow rate and gas channel geometry on the fuel cell system performance. The GDL morphology

influences greatly on the species distribution from the channel to the catalyst surface in the cell. This is expected to affect the electrochemical reaction rate that subsequently determines the fuel cell performance.

- **Chapter 5** numerically investigates the reactant gas transport in PEM fuel cells with transverse pin fins inserts in the channel flow. This is aimed at improving the system performance via effective distribution of the reactant gases at a reduced pumping power requirement penalty during fuel cell operation. A numerical optimisation tool (Dynamic-Q) was coupled with the CFD code to obtain optimum parameters required for improving PEM system performance. In this chapter, the steps involved in linking the optimisation method to a commercial CFD code are also indicated.

- **Chapter 6** numerically investigates the impact of cooling channel geometry on PEM fuel cell performance, specifically when the system is operated at higher temperatures (HT), beyond the critical temperature typical of conventional low-temperature PEM fuel cells. Optimal cooling channel geometry was obtained using a numerical optimisation algorithm. This will ensure thermal stability of the PEMFC, especially at high temperature conditions.

- **Chapter 7** provides conclusions drawn from this study, makes recommendations and discusses possible future research directions.

2

CHAPTER 2: FUNDAMENTALS OF PEM FUEL CELL SYSTEM

2.1 INTRODUCTION

In this chapter, the basic components of a PEMFC and its functions are briefly discussed. The main physical processes occurring in the fuel cell structure are discussed and the corresponding governing equations used in PEMFC modelling are also presented. Relevant equations include a basic continuity equation or conservation of mass, a momentum equation and an energy equation as applicable to fuel cells. Equations governing kinetics of electrochemical reactions in the fuel cell, charge (i.e. electrons and protons) transport in the MEA, as well as gas flux based on Darcy's diffusion formulation are also discussed. The various assumptions in the mathematical models in each fuel cell component are emphasised.

2.2 THE BASIC STRUCTURE OF A PROTON EXCHANGE MEMBRANE FUEL CELL

Figure 2.1 illustrates a simplified schematic showing basic components of a single PEMFC. The single cell (or unit cell) consists of nine different regions: the cathode current collector, the cathode channel, the cathode diffusion layer, the cathode catalyst layer, the PEM, the anode catalyst layer, the anode diffusion layer, the anode channel and the anode current collector.

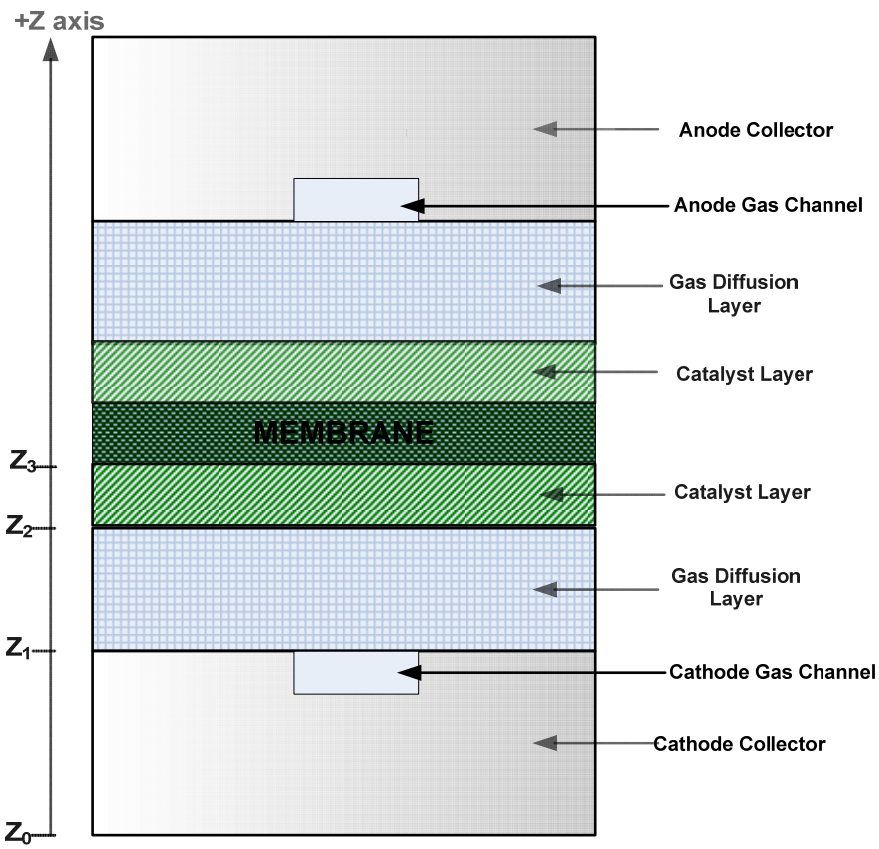

Figure 2.1 Schematic diagram of a single PEM fuel cell

A fuel cell works by catalysis mechanism, wherein electrons and protons are produced by the reactant fuels, such that the electrons are forced to travel through a circuit, thereby producing electrical power. The catalyst usually comprises platinum group metal or alloy. A similar catalytic process takes the electrons back in, combining them with the protons and the oxidant to form simple waste compound like water and heat. In a typical hydrogen-oxygen PEMFC design (Fig. 2.2), a proton-conducting polymer membrane, the electrolyte, separates the anode and cathode sides. On the anode side, hydrogen diffuses to the anode catalyst where it later dissociates into protons and electrons. These protons often react with oxidants causing them to become what is commonly referred to as multi-facilitated proton membrane (MFPM). The protons are conducted through the membrane to the cathode, but the electrons are forced to travel in an external circuit (supplying power) because the membrane is

electrically insulated. On the cathode catalyst, oxygen molecules react with the electrons (which have travelled through the external circuit) and protons to form water, the only waste product in this type of fuel cell.

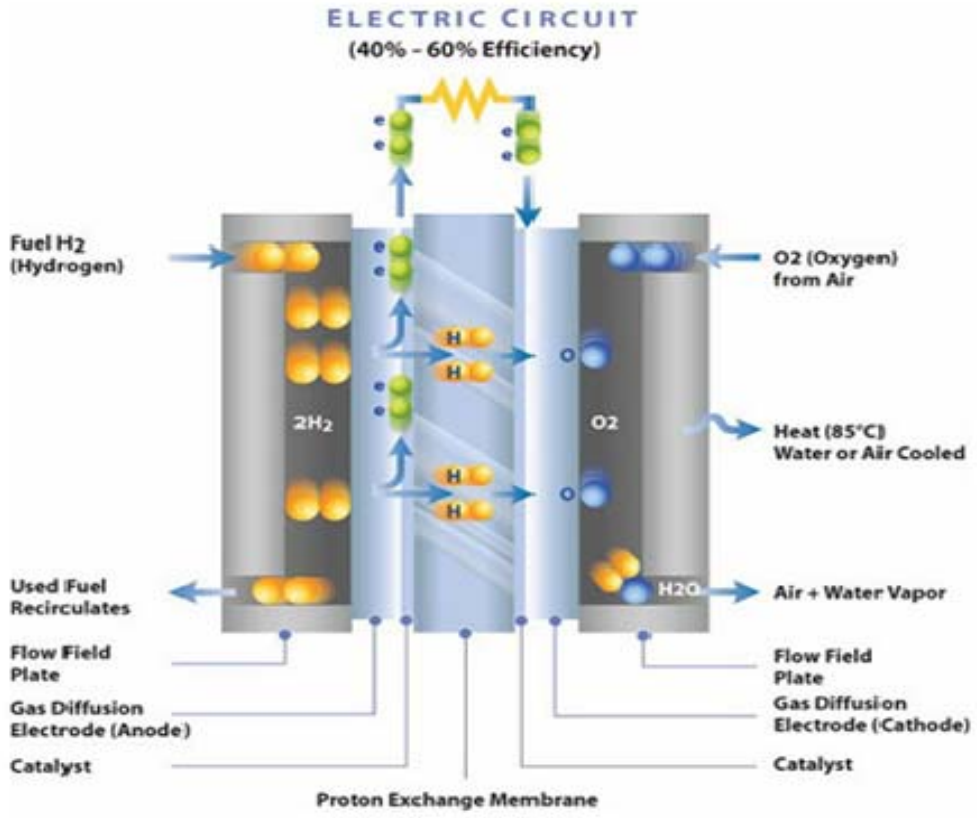

Figure 2.2 The basic structure of a PEM fuel cell showing the path of the electrochemical reaction [15]

Fuel cells are made of four major structural units. These are the following:

1. Proton Exchange Membrane (PEM),
2. Catalyst layers (anode and cathode),
3. Gas diffusion layers (anode and cathode) (GDL),
4. Bipolar plates with flow channels for reactants and coolant in larger cell stacks.

Each of these is discussed further in the following sections.

2.2.1 PROTON EXCHANGE MEMBRANE

The proton exchange membrane (PEM) functions primarily as conductor of ions, but it also serves as a separator between the reactant fuel gases, and acts as an electronic insulator. A functional PEM must also have sufficient mechanical and thermal stability during fuel cell operation. The liquid water in the PEM is transported because of convection, diffusion, dispersion, pressure gradients and electro-osmotic forces being dragged by the moving protons [101]. For effective performance of the PEM, some level of membrane hydration is necessary. However, excess water accumulation in the fuel cell electrodes can result in electrode flooding, so adequate moisture balance must be achieved within the cell.

The most common solid polymer electrolytes consist of a hydrophobic and inert polymer backbone sulfonated with hydrophilic acid clusters to provide adequate conductivity. For example, the most widely used electrolyte membranes in PEMFCs are known by their trade names and are called Nafion®. Nafion® has similar backbone structure as Teflon® but has added sulfonic acid groups [102]. In cases where the amount of water in the membrane becomes low, Nafion® conductance diminishes significantly. The membrane humidification in the fuel cell is mainly achieved through cathode reaction. Many systems utilise reactant gas humidification to maintain hydration. Modern perflourosulfonated ionomer electrolytes for hydrogen gas (H_2) PEMFCs are 18-25 μm thick with a practical operating temperature limit of 120ºC, although PEMFC operation is rarely greater than 90ºC due to adequate humidity requirements and operational lifetimes [103]. There are ongoing efforts [104, 105] to develop a high temperature membrane in order to improve the performance and efficiency of the PEMFC system.

2.2.2 CATALYST LAYERS

High activation energy is required in PEMFCs to induce electrochemical reactions. This is usually achieved by using a catalyst. The catalyst layers (CLs) are essentially

sandwiched between the ionomer membrane and a porous, electrically-conductive substrate. They are the layers where the electrochemical reactions take place (reaction zone). The most common catalyst used in PEMFCs for both oxygen reduction and hydrogen oxidation reactions is platinum. CLs in PEMFCs are made up of a porous, three-dimensional structure, with a thickness of 5-30 μm. In supported CLs, the 2-10 nm catalyst is physically supported on considerable larger, 45-90 nm carbon particles [103]. In preparation of the CLs, the most important is the surface area and not the weight, so it is important to have small platinum particles (4 nm or smaller) with a large surface area finely dispersed on the surface of the catalyst support [106].

There are two distinct ways of preparing a catalyst layer and its attachment to the ionomer membrane. Such a combination of membrane and catalyst layer is referred to as the MEA (membrane electrode assembly). The first way of MEA preparation is to deposit the catalyst layer on the porous substrate, called the GDL, typically carbon fibre paper or carbon cloth, and thereafter hot-press it to the membrane. The second method of MEA preparation is the application of the catalyst layer directly or indirectly (via a decal process) to the membrane, forming the so-called 3-layer MEA or catalysed membrane. The porous substrate may be added later, either as an additional step in the MEA preparation or in a process of stack assembly [106].

Minimising the cell potential losses due to the rate of proton transport and reactant gas permeation in the depth of the electrocatalyst layer requires making the layer relatively thin. Also, the metal-active surface area should be maximised by making the platinum (Pt) particles as small as possible. The first design requirement entails higher Pt/C ratios (>40% by wt), however smaller Pt particles and consequently larger metal areas are achieved with lower loading. In general, higher Pt loading results in an increased voltage gain [107], assuming equal utilisation and reasonable thickness of the catalyst layer. An efficient catalyst layer must have facile transport of ions, electrons, reactants and products with a high electrochemical active surface area where the reactants, catalyst, proton and electron conduction are all available.

2.2.3 GAS DIFFUSION LAYERS

The gas diffusion layer (GDL) consists of a carbon fibre or woven cloth macroporous layer and possibly a highly hydrophobic microporous layer developed to enable better electrical contact between the catalyst layer and fuel system lands. For a GDL to function efficiently in a fuel cell system, it must have the following properties [108]:

- It should be sufficiently porous to allow the flow of both reactant gases (hydrogen and oxygen) and product water. Depending on the design of the flow field, through-plane and in-plane diffusion is important.
- It must be both electrically and thermally conductive, again both through-plane and in-plane conduction are important. Interfacial or contact resistance is typically more important than bulk conductivity.
- The catalyst layer should be made of discreet small particles; hence the pores of the GDL facing the catalyst layer must be minimum.
- It must be sufficiently rigid to support the "flimsy" MEA. However, it must have some flexibility to maintain good electrical contacts.

In addition, the GDL should be able to conduct heat generated at the catalyst layers mainly by conduction to the bipolar plates and by convection in gas phases to the gas flow channels [109]. Carbon fibre based materials such as carbon-fibre papers and woven carbon fabrics or cloths are usually used, considering the conflicting array of GDL requirements. The GDL (both anode and cathode) material is typically treated with a hydrophobic material, such as Teflon, to facilitate water removal and subsequently prevent flooding in their bulk. In addition, the interface with the adjacent catalyst layer may be fitted with a coating or a microporous layer to ensure better electrical contacts, as well as efficient water transport into and out of the diffusion layer. The pores in this layer are usually between 0.1 and 0.5 μm, thus much smaller than the pore size of the carbon fibre papers (20-50 μm) [108].

2.2.4 BIPOLAR PLATES

PEM fuel cells are usually designed by connecting multiple cells in series with bipolar plates (BPPs). These BPPs structurally support the thin MEAs in PEM fuel cells and actually comprise almost all of the volume of the fuel cell stack, and typically over 60% of the weight and 30% of the total cost in a fuel cell stack [70]. The BPPs collect and conduct the current from the anode of one cell to the cathode of the next, while evenly distributing the fuel gas over the surface of the anode, and the oxygen/air over the surface of the cathode through the flow channel. In some designs, it performs the task of facilitating water and heat management. These functions are possible through the plate topologies and material composition of the BPPs. The essential requirements for BPPs, in respect of physiochemical characteristics, are efficient and uniform distribution of the reactant gases over the electrodes to minimise the concentration over potential; high values of electronic conductivity for current collection; adequate mechanical strength for stack integrity; impermeability to reactant gases for safe operation; resistance to corrosion in severe cell environment for long lifetime; cheap materials; and easy and automated fabrication for low cost [110].

In general, two families of materials have been used for PEM fuel cell BPPs, namely polymer-sealed graphite-composite and metallic. The polymer sealing is used to ensure that the normally porous graphite is impermeable to water. For high power density, low weight and robust stack design, however, metallic plates are required [103]. Technical difficulties with metal BPPs include difficulty in scaling and corrosion, which results in rapid electrolyte degradation and poor electrical contact resistance. In fuel cells, a balance exists between gas supply and current conduction. Hence, there is need for large-scale porosity in the flow fields, which requires seeking an optimal flow field design that will efficiently supply the required reactant gases at lower pumping power requirement. The effective design and optimisation of the gas flow fields and BPPs remains a pertinent explored area for reasonable cost reduction and optimum performance attainment for PEM fuel cells [111, 112].

2.3 PEM FUEL CELL STACK DESIGN

Since fuel cells operate at less than 100% efficiency, the voltage output of one cell is less than 1.16 volt. Most applications require much higher voltages than this, (for example, effective commercial electric motors typically operate at 200-300 volts), the required voltage is obtained by connecting individual single fuel cells in series to form a fuel cell stack [113]. In stack design, weight and volume is crucial. Hence, to decrease the overall volume and weight of the stack, instead of two current collectors, only one plate is used with a flow field cut into each side of the plate. This type of arrangement is referred to as bipolar plates (BPPs). The bipolar plate (BPP) separates one cell from the next, with the single plate doing dual work of carrying the hydrogen gas on one side and air on the other side. A typical stack configuration is illustrated in Figure 2.3.

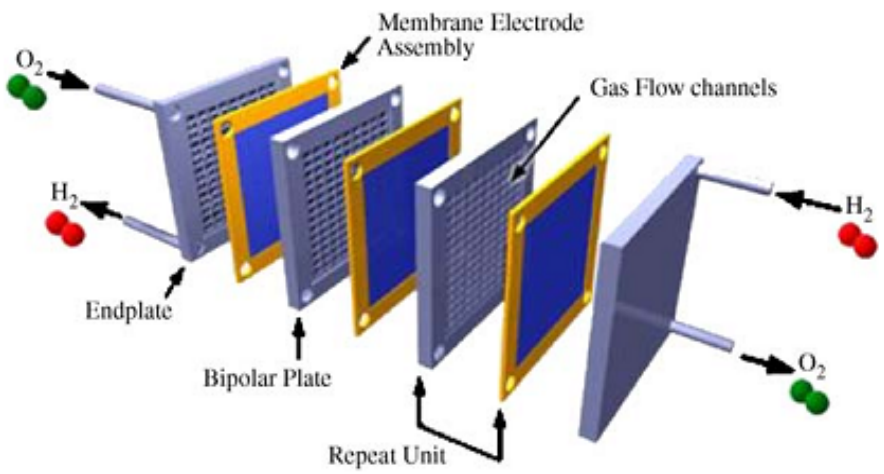

Figure 2.3 Fuel cell stack component [71]

The bipolar configuration is best suited for large fuel cells since the current is conducted through relatively thin conductive plates, thus it travels short distance through a large area. This causes minimum electroresistive losses even with the use of a relatively poor electrical conductor such as graphite (or graphite mixtures). However, for small cells it is possible to connect the edge of one electrode to the

opposing electrode of the adjacent cell by some kind of connector [113]. A good fuel cell stack design should have the following properties [103]:

1. Uniform distribution of reactants to each cell
2. Uniform distribution of reactants inside each cell
3. Minimum resistive losses (choice of materials, configuration, uniform contact pressure)
4. No leak of reactant gases (internal between the cells, or external)
5. Mechanical sturdiness (internal pressure including thermal expansion, and external forces during handling and operation, including shocks and vibrations).

Fuel cell performance is sensitive to the flow rate of the reactant gases, hence it is highly necessary that each stack receives approximately the same amount of reactant gases. Uniformity in flow distribution would result in even performance of the cell. Therefore, to achieve uniform distribution, feeding of the cell in the stack is done in parallel through a manifold that can be either external or internal. In fuel cell design, internal manifolds are commonly employed because of better sealing and versatility in gas flow configuration [113]. The reactant gases entering the fuel cell stack cell must be distributed over the entire active area. This is practically achieved through a flow field, which is basically a form of channels covering the entire area in some pattern or porous structure. The pattern of the flow field in the plate, as well as the width and depth of the channels, have a large impact on the effectiveness and the even distribution of the reactant gases across the active area of the membrane/electrode assembly. The flow field design also affects the water supply to the membrane and water removal from the cathode [113]. The following are the key flow field design variables [106]:

- flow field shape
- flow field orientation
- configuration of channels

- channels shape, dimensions and spacing
- pressure drop through the flow field

Flow field design is a critical aspect in fuel cell manufacturing and is a well-kept secret by stack manufacturers [106]. CFD modelling is a great tool for the design of fuel cell flow fields [114, 71].

2.3.1 HYDROGEN FUEL CELL SYSTEM COMPONENTS

Fuel cell stacks need to be integrated into a complete fuel cell system for it to operate. The fuel cell system must be of appropriate weight and volume to fit into the space provided for operation. The operation of the entire engine must maintain the near-zero emissions and high efficiency of the fuel cells. In addition, all these requirements must be met with components that are both inexpensive and designed for low cost, high volume manufacturing. Figure 2.4 is a schematic of typical hydrogen PEMFC system.

The hydrogen fuel cell system includes the following subsystems and control components [103]:

2.3.1.1 *Reactant storage, delivery and recycling*

This comprises of the pumps and blowers required to supply the fuel cell stack with prescribed flow rates of fuel and oxidiser and to recycle unused fuel back into the anode inlet stream. Typically, only fuel storage and recycling are needed as air is used as the oxidant.

2.3.1.2 *Humidification*

This system is required for humidification of the flow of reactant gases. Portable system designs are passively humidified, thereby eliminating this subsystem completely at the expense of reduced performance.

2.3.1.3 *Cooling*

Systems larger than 1 kW power typically require active cooling of the stack to remain within membrane material tolerances and achieve uniform system performance. Smaller, low-portable systems can be passively cooled. The choice of coolant is an active area of research. Distilled water can be used but will freeze at subzero temperatures. Ethylene glycol is the coolant of choice for contemporary automotive applications and can operate at subzero temperatures, but contact with electrolytes can result in irreversible damage.

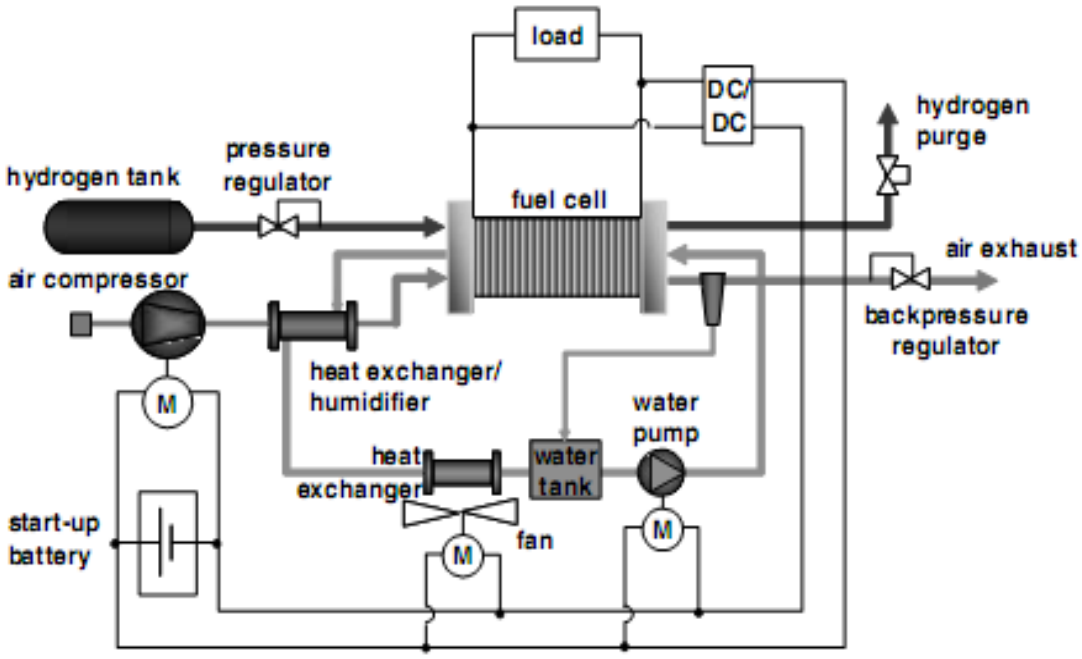

Figure 2.4 A schematic of a complete hydrogen-air fuel cell system [115]

2.3.1.4 *Hydrogen reformation*

In some fuel cell systems, hydrogen fuel is obtained from liquid hydrocarbon or alcohol fuel. This fuel cell type requires a hydrogen generation system. For stationary applications, a fuel reformer is often incorporated. Meanwhile, in automobile or

portable applications, on-board reformation is typically avoided due to the required excessive complexity, cost and transient control limitations.

2.3.1.5 *Power conditioning and control*

Power output from a fuel cell stack is normally in the form of direct current (DC) which must be inverted to alternating current (AC) and conditioned into a suitable voltage range to power equipment. The fuel cell control system is responsible for all system monitoring and maintenance of stable and safe operation through feedback from a variety of flow, pressure, voltage, current and temperature sensors [103].

2.3.1.6 *Startup Power System*

External power inputs are usually incorporated to assist in the system startup. An auxiliary high-power battery to run pumps and heaters during startup, or to provide power to overcome voltage transients and reversals in the fuel cell stack is often required.

2.3.1.7 *System Humidification*

Fuel cells have a precarious balance between a moist electrolyte needed for high ionic conductivity and a flooded cell that degrades fuel cell performance. It is possible that some sections of the same fuel cell or individual plates in a stack will be critically dry and other sections in the cell or different plates in a stack will be flooded. Hence, some humidification is typically required at the inlet of the fuel cell to ensure adequate performance. In addition, strong humidity gradients in the electrolyte can result in internal stresses that limit system durability. Humidification in fuel cell is basically achieved by two main procedures, *passive approach* and *direct approach*. In the former, the water generated by the reaction in the cell is used to maintain a proper

moisture balance and humidity of the incoming reactant flow without external power. However, in active humidification, a separate humidifier is directly employed to provide the humidification of the incoming flow with stored or recycled water.

2.4 THEORIES OF TRANSPORT AND ELECTROCHEMICAL PROCESSES IN PEMFCs

Understanding the transport, electrochemical and coupled spontaneous oscillations of hydrodynamic processes in the fuel cell system requires the understanding the physics of the various processes within the fuel cell structures. The transport and electrochemical processes of a typical PEMFC (Figure 2.1) are discussed below:

- The hydrogen fuel is supplied through the anode gas flow channel and is distributed to the thin catalyst layer section of the fuel cell via the anode GDL.
- The oxidation of the hydrogen molecules occur in the anode catalyst layer to produce protons and electrons which, in turn, are transported to the cathode through the fuel cell membrane and an external circuit, respectively.
- In the cathode catalyst layer, the oxidant molecules (transported from the cathode gas flow channel and GDL) combine with the protons and the electrons from the anode section to produce water.

The basic half-cell reaction occurring in the fuel cell is given as:

anodic: $$H_2 \rightarrow 2H^+ + 2e^-, \tag{2.1}$$

cathodic: $$\frac{1}{2}O_2 + 2H^+ + 2e^- \rightarrow H_2O \text{ , and} \tag{2.2}$$

net-reaction: $H_2 + \frac{1}{2}O_2 \rightarrow H_2O$. (2.3)

From equation 2.3, one of the key advantages of the fuel cells is seen. That is that the only by-product of the reaction is water, which is non-pollutant to the environment compared to the harmful products of combustion using fossil fuels.

Modelling transport and electrochemical processes taking place in the various layers in the fuel requires solving five types of constitutive relations simultaneously: (i) the conservation equations, (ii) constitutive relations for various fluxes, (iii) kinetic equations for reactions, (iv) equilibrium relationships and (v) auxiliary relations such as variable definitions and Faraday's Law [25]. The conservation equations are applicable to all the layers in the fuel cell, while the other four equations are related specifically to sections within the fuel cell: membrane, GDL and the catalyst layers.

2.4.1 CONSERVATION EQUATIONS

The fundamental description of fuel cell operation involves the five conservation principles, namely, mass, momentum, species, electrical charge and thermal energy. Generally, unified and individual modelling approaches are used in fuel cell modelling. These two approaches are used in the present work and have been elaborately discussed by Yang and Pitchumani [116]. A brief discussion on these approaches is presented in this section. A unified-domain approach allows a valid set of governing equations for all the fuel cell layers written in vector form as [117, 118]:

mass: $$\frac{\partial(\varepsilon\rho)}{\partial t} + \nabla \cdot (\rho \mathbf{u}) = S_m \,, \tag{2.4}$$

momentum: $$\frac{1}{\varepsilon}\left[\frac{\partial(\rho \mathbf{u})}{\partial t} + \frac{1}{\varepsilon}\nabla \cdot (\rho \mathbf{u} u)\right] = -\nabla p + \nabla \cdot \tau + S_u \,, \tag{2.5}$$

species: $$\frac{\partial(\varepsilon C_k)}{\partial t} + \nabla \cdot (\mathbf{u} C_k) = \nabla \cdot \left(\mathbf{D}_k^{eff} \nabla \mathbf{C}_k\right) + S_k \,, \tag{2.6}$$

charge: $$\nabla \cdot \left(\boldsymbol{\kappa}^{eff} \nabla \boldsymbol{\Phi}_e\right) + j = 0 \,, \tag{2.7}$$

$$\nabla \cdot \left(\boldsymbol{\sigma}^{eff} \nabla \boldsymbol{\Phi}_s\right) - j = 0 \,, \tag{2.8}$$

and finally,

energy: $$\frac{\partial\left[(\rho c_p)_m T\right]}{\partial t} + \nabla \cdot (\rho c_p \mathbf{u} T) = \nabla \cdot \left(k^{eff} \nabla T\right) + S_T \,. \tag{2.9}$$

The unified-domain approach eliminates the requirement of prescribing assumed or approximate boundary conditions at the interfaces between the various layers of the fuel cell system. The main assumptions made in the conservation equations are: (i) the reactant gases are an ideal gas mixture and (ii) flow is incompressible and laminar due to small flow velocities occurring in the fuel cell system. The dependent variables $\mathbf{u}$, p, $\boldsymbol{C}_k$, Φ_e, Φ_s, and T in the equations denotes the superficial fluid velocity vector, pressure, molar concentration of species k, electrolyte (membrane) phase potential, solid phase potential, and temperature, respectively. The solid phase relates to the electron conducting materials in the fuel cell system, *i.e.,* the flow channel BPPs, the GDL, or the electrocatalyst and its carbon support in the catalyst layer section. In the succeeding section below, other individual equations and the description of their parameters are presented:

2.4.1.1 ***The mass equation (equation 2.4):***

In this equation, t and ε are the time and porosity, respectively, and the density of the gas mixture ρ is given by:

$$\rho = \sum_k MW_k C_k \ , \tag{2.10}$$

where MW_k is the molecular weight of species *k,* and the summation is performed over all the gas species involved. The source term S_m assumes non-zero value at the catalyst layers, resulting from the consumption/production of electrochemical reactions as well as diffusion and osmotic drag of water through the membrane [117]:

$$S_m = -MW_{H_2} \frac{j_a}{2F} + MW_w \left[\nabla \cdot \left(D_{w,m} \nabla C_w - n_d \frac{i_e}{F} \right) \right], \text{ for anode} \tag{2.11}$$

and

$$S_m = -MW_{o_2} \frac{j_c}{4F} + MW_{H_2} \frac{j_c}{2F} - MW_w \left[\nabla \cdot \left(D_{w,m} \nabla C_w - n_d \frac{i_e}{F} \right) \right], \text{ for cathode,} \tag{2.12}$$

where $D_{w,m}$ is the liquid water diffusion coefficient in the membrane, and n_d is the electro-osmotic drag coefficient. The current density in the membrane (resulting from proton flux), i_e, is related to the membrane phase potential, Φ_e, through Ohm's law [71]:

$$\mathbf{i}_e = -\boldsymbol{\kappa}^{eff} \nabla \boldsymbol{\Phi}_e \ , \tag{2.13}$$

where $\boldsymbol{\kappa}^{eff}$ is the effective proton conductivity in the catalyst layer. The current density in the solid phase, $\mathbf{i}_s$, could also be obtained by using Ohm's law as [116]:

$$\mathbf{i}_s = -\sigma \nabla \boldsymbol{\Phi}_s \ , \tag{2.13b}$$

where σ is the electrical conductivity.

2.4.1.2 ***The momentum equation (equation 2.5):***

The effect of porous media is represented by the source term, $S_u = -\mu \mathbf{u}/K$ wherein μ and K denote viscosity and hydraulic permeability, respectively. In the porous layers (*i.e,* the GDLs, hydraulic layers and membrane), the viscous term from the divergence of the viscous stress, $\nabla \cdot \boldsymbol{\tau}$, and the inertial terms may be small and the momentum equation is reduced to Darcy's law [116].

2.4.1.3 ***The species equation (equation 2.6):***

The equation denotes the reactant species diffusion in the fuel cell system. The first term on the right-hand side of the equation indicates that the species diffusion is modeled by Fick's law for a binary mixture, which is an acceptable approximation for multicomponent diffusion in PEM fuel cells [117]. The effective diffusivity for species k is adopted to account for the effects of porous media, and the expression D_k^{eff} represents the effective diffusion coefficient for the species. The source term S_k for hydrogen and oxygen species is due to the electrochemical reactions, which may be written in general form as [117]:

$$\sum_k v_k M_k^z = ne^- \quad , \tag{2.14}$$

where v, M_k and exponent z are the stoichiometric coefficient, the chemical symbol, and charge number for species k, respectively, and n depicts the number of electrons transferred across the charge double layer. The consumption rate of the reactant species, S_k, is related to the volumetric transfer current, j, through Faraday's law [116]:

$$S_k = -\frac{v_k j}{nF} \ , \tag{2.15}$$

with j given by the Butler-Volmer equation [118]:

$$j = A_{av} i_o \left[\exp\left(\frac{2\alpha_a F}{RT} \eta \right) - \exp\left(-\frac{2\alpha_c F}{RT} \eta \right) \right], \tag{2.16}$$

where A_{av} is the electrochemically active area per unit volume, i_o is the exchange current density, and F is the Faraday's constant. The anodic and cathodic charge transfer coefficients, α_a and α_c, represent the portion of the electrical energy harnessed in driving the electrochemical reactions, and the values are between 0 and 1, depending on the reactions and material properties involved. The activation overpotential, η, is defined as:

$$\eta = \Phi_s - \Phi_e - U_0 \ , \tag{2.17}$$

where U_0 is the thermodynamic equilibrium potential, which is determined by using the Nernst equation for the cathode reaction [119]:

$$E = E^0 + \frac{RT}{2F} \ln\left(\frac{a_{H_2} \cdot a_{O_2}}{a_w} \right), \tag{2.18}$$

where E^0 is the electromotive force (emf) at the standard pressure (*i.e.,* 1 bar), R is the universal gas constant, T is the temperature, F is the Faraday constant, and a_{H_2} a_{O_2}, and a_w are the activities of the hydrogen, oxygen, and water species, respectively. The effect of osmotic drag is also added to the source S_k for the water species in the catalyst and membrane layers [117].

2.4.1.4. *The charge transport equations (Equations 2.7 and 2.8):*

These equations involve the volumetric transfer current, *j,* as a source term. The general Butler-Volmer equation, Eq. (2.16), may be simplified for the anode and cathode catalyst layer depending on the characteristic of the half-cell reactions [117, 120]:

anode: $$j_a = A_{av} i_{0,a}^{ref} \left(\frac{C_{H_2}}{C_{H_{2,ref}}} \right)^{1/2} \left(\frac{\alpha_a + \alpha_c}{RT} F \eta_a \right) \text{ and} \tag{2.19}$$

cathode: $$j_c = A_{av} i_{0,c}^{ref} \left(\frac{C_{O_2}}{C_{O_{2,ref}}} \right) \exp\left(-\frac{\alpha_c}{RT} F \eta_c \right), \tag{2.20}$$

where the sub/superscripts *a, c,* and *ref ,* denote the anode, cathode and reference state, respectively. The hydrogen oxidation reaction (HOR) in the anode catalyst layer is fast and the overpotential η_a is typically small, and j_a in Eq. (2.19) is approximately proportional to η_a. In cases where the PEM fuel cell operates on a reformate feed at the anode section, the electrochemical reactions in the anode catalyst layer involve the adsorption process of CO, leading to a decreased active area, A_{av}, at the anode section of the fuel cell [121, 122]. The oxygen reduction reaction (ORR) is typically slow with high η_c, and the expression for j_c, Eq. (2.20), may be obtained by neglecting the anodic reaction term of Eq. (2.16).

2.4.1.5 *The energy equation (Equation 2.9):*

In the energy equation, K^{eff} is the thermal conductivity, and the heat capacitance in a porous material, $(\rho c_p)_m$, is a volume-averaged volumetric specific heat over the solid matrix and the fluid in the micropores:

$$\left(\rho c_p\right)_m = \varepsilon\left(\rho c_p\right) + \left(1-\varepsilon\right)\left(\rho c_p\right)_s , \tag{2.21}$$

where the subscript *s* refers to the solid material and $\left(\rho c_p\right)$ pertains to the fluid.

The source term S_T in Eq. (2.9) consists of contributions from three mechanisms, *i.e.,* irreversible heat from the electrochemical reaction, reversible or entropic heat, and Joule heating. In solving the conservation equations discussed in this section, the material property characterisation (*i.e.,* transport properties of the membrane, kinetic data for electrochemical reactions, effective parameters for porous materials, and properties of the reactants and products) must be considered.

2.4.2 MODELS OF INDIVIDUAL PEM FUEL CELL COMPONENTS

The previous discussion focuses on the simulation of entire fuel cell systems. The subsequent discussion will focus on numerical models specific to individual cell components such as cell membrane, GDLs, etc.

2.4.2.1 *Membrane models*

The membrane model discussed here will focus primarily on the two major types of macroscopic models of the membrane, namely, the single phase and the two-phase models. The membrane is one of the most important components of a PEM fuel cell, which serves to effectively separate the anode fuel from the cathode oxidant and to conduct protons at high rates during cell operation. The discussions here focus on the Nafion membrane, owing to the fact that the governing equations for Nafion are generally valid for other types of membranes (only with different property values) [116]. Most macroscopic models consider a membrane consisting of three species: the membrane polymer, proton and water. Other types of ions are neglected in the three-species system [123].

(i) Single-phase models

The single-phase model (or diffusive) considers the vapor-equilibrated membrane. The system is treated as a single, homogeneous phase where the water and proton dissolve in the polymer matrix and is transported by diffusion. The membrane matrix is considered to be stationary in the space, and the fluxes of the dissolved species may be obtained by the dilute solution theory [124] or concentrated solution theory [125, 126]. The dilute solution theory considers only the interactions between each dissolved species and the solvent (i.e., the polymer matrix), and the general motion of charged carriers is governed by the Nernst-Planck equation [116]:

$$\mathbf{N}_{\mathrm{i}} = -z_i u_i F c_i \nabla \Phi_e - D_i \nabla c_i + c_i v_e \ . \tag{2.22}$$

In Eq. (2.22), the first term represents the migration of the charged particles *i* in an electrolyte potential gradient $\nabla \Phi_e$, where z_i is the charge number, and u_i and c_i are the mobility and concentration, respectively. The diffusive and convective fluxes are governed by the second and the third term, respectively, and the diffusion coefficient D_i is related to the mobility u_i by the Nernst-Einstein equation [124]:

$$D_i = RTu_i \ . \tag{2.23}$$

Since the one-phase analysis considers the polymer matrix as stationary solvent, the convective velocity $\boldsymbol{v}_e = 0$, Eq. (2.22) reduces to Ohm's law (*i.e*, Eq. (2.13)) for the case of zero proton concentration gradient, and to Fick's law when $z_i = 0$ in the case of water transport.

The flux of the proton across the membrane induces a flow of water in the same direction via the electro-osmotic drag effect. The electro-osmotic flow is a result of

the proton-water interaction which cannot be modelled by the dilute solution theory. The three-species membrane system is better modelled using the concentrated solution theory, which accounts for the interaction among all the species. Considering the thermodynamic driving force to be a sum of frictional interactions among different species, the following expressions for the ionic and water fluxes are obtained [125, 126]:

$$i_e = -\frac{-\kappa n_d}{F}\nabla\mu_w - \kappa\nabla\Phi_e \quad \text{and} \tag{2.24}$$

$$N_w = n_d\frac{\boldsymbol{i}_e}{F} - \alpha_w\nabla\boldsymbol{\mu}_w \ . \tag{2.25}$$

where μ_w and α_w , respectively, denotes the chemical potential and transport coefficient of water. The proton-water interaction is taken into account by the two terms containing the electro-osmotic drag coefficients, n_d , in each of Eqs. (2.24) and (2.25).

(ii) Two-phase models

The two-phase model, also known as the hydraulic model, considers the liquid membrane to consist of two-phases, namely, the polymer matrix and the liquid water. A major assumption concerning two-phase models is the fully hydrated state of the membrane, corresponding to the complete filling of the membrane micro-pores with liquid water. This implies that concentration gradient and the diffusion transport of the liquid water species should be zero. The proton species is assumed to be dissolved in water and moves along with the water molecules. Bernadi and Verbrugge [23, 127] presented one of the first two-phase models and adopted the Nernst-Planck equation, Eq. [2.22], to describe the proton flux. The convective velocity, $\mathbf{V}_w$, is non-zero and is given by Schlogl's equation for the water species [25, 128], that is,

$$\mathbf{V}_w = -\left(\frac{K}{\mu}\right)\nabla p_L - \left(\frac{K_\Phi}{\mu}\right) z_f c_f F \nabla \Phi_e \ , \tag{2.26}$$

where K and K_Φ represent the effective hydraulic and electrokinetic permeability, respectively, p_L is the liquid pressure, μ is the liquid viscosity, and z_f and c_f denote the charge and concentration of fixed ionic sites, respectively. In two-phase models, the water flux is attributed to the combined effects of a potential and a pressure gradient. The portion of water flux driven by the pressure gradient is primarily due to the permeation of water through the micro-pore network of a fully hydrated membrane. When the membrane is partially hydrated, water concentration gradients exist across the membrane thickness and a modification of the hydraulic models becomes necessary.

2.4.2.2 *Gas diffusion layer models*

The GDL is the porous diffusion media between the catalyst layer and the gas channel. It provides structural support, uniform distribution of the reactant gases, and a pathway for electrons and liquid water to or from the catalyst layer. Due to the high conductivity of carbon in the gas diffusion layer, the conduction of electrons is usually ignored in most GDL models. However, the electronic conduction may become an important factor for the current distribution due to small contact areas with the gas channels [129] or the composition of the diffusion media [36]. Ohm's law accounting for porous media effect is adopted for the electrical current, $\boldsymbol{i}_s$, in the GDLs:

$$\boldsymbol{i}_s = -\sigma^{eff}\nabla\mathbf{\Phi}_s = -\frac{\varepsilon_s}{\tau_s}\sigma_0\nabla\mathbf{\Phi}_s = -\varepsilon_s^{1.5}\sigma_0\nabla\mathbf{\Phi}_s \ , \tag{2.27}$$

where σ^{eff} depicts the effective conductivity of the porous GDL, σ_0 is the intrinsic conductivity of the GDL material, and ε_s and τ_s are the volume fraction and tutorsity of the solid conducting phase, respectively. With the assumption of one-dimensional steady-state flow, the fluxes of the various reactants in the GDLs are constant and are related to the current density by the stoichiometric coefficients [130, 131]. However, the water flux may not be constant due to evaporation or condensation in the porous media. A rate term for the phase change, r_w, may be written as [130]:

$$r_w = h_m\left(\rho_w^{sat} - \rho_w\right) = Sh\frac{D_{vg}^{eff}}{L} f_e\left(\rho_w^{sat} - \rho_w\right), \tag{2.28}$$

where h_m is the mass transfer coefficient, ρ_w is the partial density of water vapor and ρ_w^{sat} is the saturation partial density of water, which may be correlated for the pore effects via the Kelvin equation [132]. The mass transfer coefficient, h_m, is related to the Sherwood number, Sh, via the correlation:

$$h_m = Sh\frac{D_{vg}^{eff}}{L} f_e, \tag{2.29}$$

where L is the characteristic length scale, D_{vg}^{eff} is the effective diffusion coefficient of water vapor, and f_e is the specific area of the liquid/vapor interface. In the GDL, it is evident that two-phase flow existed. These are gas and liquid water phase flow, which are further discussed hereafter.

(i) Gas-phase transport in gas diffusion layers

The transport of a multicomponent gas mixture through a porous media is usually described by the Stefan-Maxwell equations [133]:

$$\nabla x_i = \sum_j \frac{x_i \mathbf{N}_j - x_j \mathbf{N}_i}{c_T \mathbf{D}_{ij}^{eff}} \quad , \tag{2.30}$$

where x_i and N_i are the mole fraction and the molar flux of species i, respectively, c_T is the total concentration or molar density of all the gas species, and D_{ij}^{eff} is the effective binary diffusion coefficient for species i and j, which may be related to the binary diffusion coefficient D_{ij} via the Bruggeman relation:

$$\boldsymbol{D}_{ij}^{eff} = \varepsilon_G^{1.5} \boldsymbol{D}_{ij} \quad , \tag{2.31}$$

where ε_G denotes the volume fraction of the gas phase, and equals to the bulk porosity of the media when the liquid water is ignored. In the case of two-phase flow, ε_G must be determined from the liquid saturation condition in the GDL. With a decrease in pore size in the GDL, the gas molecules collide more often with the pore wall than with each other, resulting in Knudsen diffusion from the intensified gas-wall interaction [134]. From an order-of-magnitude analysis, it is noted that the bulk diffusion dominates when the mean-free path of a molecule is less than 1% of the pore radius, while Knudsen diffusion dominates when the mean-free path is more than 10 times the pore radius [134]. In accounting for the gas-wall interaction, a Knudsen diffusion term is added to the Stefan-Maxwell equation based on a dusty-gas analysis [135]:

$$\nabla x_i = -\frac{\mathbf{N}_i}{c_T \mathbf{D}_{k_i}^{eff}} + \sum_j \frac{x_i \mathbf{N}_j - x_j \mathbf{N}_i}{c_T \mathbf{D}_{ij}^{eff}} , \tag{2.32}$$

where the effective Knudsen diffusion coefficient $D_{k_i}^{eff}$ is proportional to the mean pore radius, r_p, and the mean thermal velocity of the gas molecules [136]:

$$D_{k_i}^{eff} = \frac{2}{3} r_p \sqrt{\frac{8RT}{\pi MW_i}}, \tag{2.33}$$

where *R, T, and* MW_i are the gas constant, temperature, and molecular weight of species *i,* respectively.

Most models treat the gas transport in the GDL as a pure diffusion problem where total gas pressure remains constant through the thickness of the porous media whereas, in computational fluid dynamics (CFD) models the average convective velocity, $\boldsymbol{v}_G$, is computed by adopting Darcy's law for the gas phase [133]:

$$\boldsymbol{v}_G = -\frac{K_G}{\mu_G} \nabla p_G, \tag{2.34}$$

where K_G and μ_G are the permeability and viscosity for the gas mixture, respectively, and most computational fluid models incorporate Eq. (2.34) as a source term into the momentum equation.

Generally, the pressure difference through the GDLs from most simulation results is small and the assumption of uniform pressure may be valid for typical operating conditions [127, 137]. This observation is not totally unexpected, since the gas mixture has convective flow in the channel direction and transportation is only feasible through the porous by diffusion due to a no-slip condition at the pore walls.

(ii) Liquid Water Transport in Gas Diffusion Layers

Liquid water transport is critical to cell performance. Sufficient liquid water is desirable for high membrane conductivity, while excessive liquid may block the pores in the GDL, preventing the reactants from reaching the reaction sites. In some simplified models, liquid water is treated as a stationary species that occupies a

certain volume fraction in the GDL pores [31, 138]. The effective binary diffusivities are thus decreased (see Eq. 2.31) and the flooding effect of liquid is accounted for to some extent. Most of the simplified models use the liquid volume fraction as a fitting parameter [31]. More elaborate models treat the liquid water to be fine droplets that flow with the gas mixture [83, 139]. Evaporation and condensation may take place, however, a separate liquid phase is not considered. In these models, the liquid is assumed to be a component of the gas and exerts negligible influence on the gas flow field. The models keep track of the liquid water volume fraction at various locations without resulting in complicated two-phase transport analyses.

The two types of models mentioned above essentially describe single-phase transport, while more accurate treatment of liquid water flow requires two-phase flow models. To account for liquid water flux, some simple two-phase models assume isolated gas and liquid pores in the media [130, 127, 140]. This assumption is based on the fact that the GDL is a mixture of hydrophobic Teflon and hydrophilic carbon solid. The flux of liquid water follows from Darcy's law:

$$\mathbf{N}_{w,L} = -\frac{K}{V_w \mu} \nabla p_L \ , \tag{2.35}$$

where the subscript L denotes the liquid phase and V_w is the molar volume of water. However, some models adopted a phase mixture approach where all the properties pertain to a gas-liquid mixture [141, 142]. These models use Eq. (2.35) to perform liquid flux computation, which is omitted by the single-phase models. An oversimplification in this approach is that the liquid flows with the same velocity as the gas, consequently, the interaction between the gas and the liquid is not adequately accounted for.

Gas-liquid two-phase flow in porous media is a well-known problem in a wide range of engineering applications, and rigorous modeling of the phenomenon has been

reported in the literature [143, 144]. Here, we restrict our discussion to gas-liquid diffusion in fuel cells. Thus, the interaction between the gas and the liquid is characterised by a capillary pressure, p_C, defined as [145]:

$$p_C = p_L - p_G = -\frac{2\gamma\cos\theta}{r} \quad , \tag{2.36}$$

where γ is the surface tension of water, θ is the contact angle of a water droplet with a pore wall, and r is the pore radius. Depending on the wetting characteristic of the GDL material, the contact angle has a range of $\theta^o \le \theta \le 90^0$ for a hydrophobic material, and $90^o \le \theta \le 180^o$ for a hydrophilic one. An important goal of the two-phase models is to predict the distribution of liquid saturation, s, which is defined as the portion of pore volume filled with liquid. Thus, the volume fraction of the gas phase, ε_G, is related to the porosity of the GDL, ε_0 as:

$$\varepsilon_G = \varepsilon_0(1-s). \tag{2.37}$$

The equation implies that the increase in saturation results in a decrease in gas phase volume fraction and effective diffusion coefficients (Eq. 2.37). In determining the liquid saturation, s, empirical constitutive equations are adopted to relate the capillary pressure, p_C, to the saturation, s [146, 147]. Wang and Cheng [147] gave a correlation for p_C as a function of s. Thus,

$$p_C = \gamma\cos\theta\left(\frac{\varepsilon_0}{K}\right)^{0.5}\left[1.417(1-s) - 2.120(1-s)^2 + 1.263(1-s)^3\right], \tag{2.38}$$

where the surface tension is taken to be 0.0625 Nm^{-1} for the liquid water-air system at 80°C and K is the effective permeability of the GDL. The functional form for the

$p_C - s$ relationship is also determined using a bundle-of-capillary model [145]. The capillary pressure in Eq. (2.38) at various locations in the porous media must be known to determine the liquid saturation. In typical two-phase flow models, Darcy's law [Eqs. (2.34) and (2.35)] is employed to calculate the pressure fields for both liquid and gas phases, and subsequently utilised in Eqs. (2.36) and (2.38) to obtain the liquid saturation distribution. In some models, capillary pressure is used as the driving force for the liquid-water flow [148]:

$$\mathbf{N}_{w,L} = -\frac{K}{V_w \mu}\nabla p_L = -\frac{K}{V_w \mu}(\nabla p_G + \nabla p_C) = -\frac{K}{V_w \mu}\nabla p_C \,. \tag{2.39}$$

The rightmost expression in Eq. (2.39) assumes that the gas pressure is constant within the GDL. The effective permeability K in Eqs. (2.38) and (2.39) is commonly related to a relative permeability, K_r, as:

$$K = K_r K_{sat} \,, \tag{2.40}$$

where the permeability at complete saturation, K_{sat}, depends only on the structure of the porous medium. Many empirical relations existed in the literature for K_r as a function of the saturation. Some adopts a linear dependence of K_r on saturation [149, 150]. Most other models represent the relative permeabilities for liquid and gas phases, namely, K_{rl} and K_{rg}, with the following expressions [146]:

$$K_{rl} = s^3 \text{, and} \tag{2.41}$$

$$K_{rg} = (1-s)^3 \,. \tag{2.42}$$

The constitutive relations in Eqs. [2.36-2.42] is commonly incorporated in the multiphase model to simulate two-phase flow in the PEM fuel cells [146, 147].

2.4.2.3 *Catalyst layer models*

The catalyst layer is a critical component of a fuel cell. The physical processes in a catalyst layer include the electron conduction in the solid phase; the proton transport in the membrane phase; the gas diffusion in the gas, liquid and membrane phases; and the electrochemical reactions on the active catalyst sites. The HOR occurs in the anode catalyst layer and the ORR takes place in the cathode catalyst layer.

Models that are often used for the catalyst layer are either microscopic or macroscopic. The macroscopic model is classified into four different types, namely, (i) the interface model that treat the catalyst layer with zero thickness, (ii) the macrohomogeneous approach, (iii) the film models, and (iv) the agglomerate models. The catalyst models are usually for the cathode, due to the fact that the cathode reaction is slower and contributes to the principal losses in the fuel cell. However, the modelling approaches for the cathode are generally applicable to the anode catalyst layer, with only different kinetic expressions and values of properties.

(i) Microscopic models

The microscopic model is further divided into gas pore models [151, 152] and the flooded-agglomerate models [153, 154]. Since the two modelling approaches are very similar, only one, that is, the flooded-agglomerate model will be presented here. In this model, the catalyst layer is made up of a number of porous cylinders flooded with the electrolyte. The species diffusion and reaction occur within the cylinders [155]. During fuel cell operation, reactant gas diffuses through the gas pore, dissolves and diffuses in the electrolyte contained in the agglomerates, and reacts on the active sites

of the catalyst particles. The diffusion of the reactant gas is governed by Fick's law with a source term accounting for the simultaneous bulk reaction [155]:

$$D_m^{eff}\frac{\partial^2 C(r)}{\partial r^2}+D_m^{eff}\frac{1}{r}\frac{\partial C(r)}{\partial r}-S_k=0, \tag{2.43}$$

where D_m^{eff} is the effective diffusion coefficient of the dissolved species and $S_k=\frac{\nu_k j}{nF}$ is the consumption rate given by Eq. (2.15). The activation overpotential, η, in the source term S_k, is a function of *x*, and may be obtained from Ohm's law expressed as:

$$\frac{d^2\eta}{dx^2}=\frac{2nFD_m^{eff}}{K^{eff}r_0}\left(\frac{\partial C}{\partial r}\right)_{r=r_0}, \tag{2.44}$$

where K^{eff} is the effective ionic conductivity. Equation (2.44) could be solved numerically to obtain the radial distribution of current density at various locations. Subsequently it can be used to evaluate the performance of the electrode as a function of physical properties such as the intrinsic activity of the catalyst, agglomerate size, internal porosity and active surface area.

(ii) Macroscopic models

The macroscopic model is classified into different types and each is discussed below:

- *Interface models:* This model treats the catalyst layer as an infinitely thin interface between the GDL and the membrane. It is used in fuel cell simulations when the emphasis is not on the catalyst-layer but rather on the membrane, the water balance, or the nonisothermal effects. The catalyst is treated as a location where

the reactants are consumed and the water is produced especially in models focusing on water management [156, 157].

Faraday's law, Eq. (2.15), is used in the boundary conditions for the mass balance of each species between the membrane and the GDL. The overall polarisation behaviour, as a function of the catalyst interface, is also studied by using this model [138, 158]. Generally, the interface model assumes that the values of the relevant variables are constant across the thickness of the catalyst layers, based on the fact that the layers are extremely thin. However, detailed treatment of the catalyst layer is required when the structure parameters of the layer, such as the catalyst loading, need to be optimised.

- *Macrohomogeneous and thin film models:* In this model framework, the catalyst layer is assumed to consist of a uniformly-dispersed carbon-supported catalyst and the ionomer electrolyte without the gas pores. The gas species dissolve and diffuse in the membrane phase and, consequently, the diffusion rate is low. In the thin film model, gas pores are assumed to exist and the catalyst particles are covered by a thin film of electrolyte polymer. The macrohomogeneous models [159] and the thin film models ignore the microstructural details and share similar governing equations. The major distinction between the two models is the values of the diffusion coefficients, since the reactant gas diffuses in different phases, namely, in the gas phase for the thin film models and in the membrane phase for the macrohomogeneous models. A one-dimensional macrohomogeneous model for a cathode catalyst with thickness δ_{cat} is summarized in Ref. 159 and is presented here for completion. In the model, the oxygen flux, No_2 through the catalyst thickness is determined by Fick's law of diffusion:

$$\frac{dCo_2}{dx} = -\frac{No_2}{D_{o_2}^{eff}} = \frac{i(x) - I_o}{4FD_{o_2}^{eff}} , \tag{2.45}$$

where $D_{o_2}^{eff}$ is the effective oxygen diffusion coefficient, $i(x)$ is the local proton current density, and I_0 is the total current density through the cell. The solid phase is considered to be equipotential (i.e., $\Phi_s = 0$), since the ohmic losses are negligible in the highly conductive materials. Consequently, the local electrode potential, $\eta(x)$, defined as the potential difference between the membrane and solid phase, is only determined by the local electrolyte potential. Thus,

$$\eta(x) = \Phi_e - \Phi_s = \Phi_e(x). \tag{2.46}$$

Ohm's law for the conduction of protons in the ionomer phase yields:

$$\frac{d^2\eta(x)}{dx^2} = \frac{d^2\mathbf{\Phi}_e(x)}{dx^2} = \frac{j_c(x)}{\boldsymbol{\kappa}^{eff}} \quad , \tag{2.47}$$

where $j_c(x)$ is the volumetric transfer current and κ^{eff} is the effective proton conductivity. The effect of the effective oxygen diffusion coefficient $D_{0_2}^{eff}$ and effective proton conductivity κ^{eff} on the cathode performance could be obtained through Eqs. (2.46) and (2.47). Also both $D_{0_2}^{eff}$ and κ^{eff} are functions of the membrane in the catalyst layer, hence the model could be used to determine an optimal membrane gradient that significantly improves the cathode performance via optimising both the oxygen diffusion and proton transport [159].

- *Agglomerate models:* The macrohomogeneous and thin film models deal with the transport processes on macroscale across the layer thickness, while neglecting the variation of physical variables in the local agglomerate-scale. To investigate the effect in changes in the agglomerate or pore-scale on the accuracy of the modeling of the phenomenon, the characteristic length of the pore-agglomerate must be compared with the diffusion lengths, *i.e.*, the distances over which the physical

variables related significantly to the transport process change. The characteristic pore scale lengths of a PEMFC are in the range 10^{-7} to 10^{-8} m, while the diffusion lengths for the reactants in the electrolyte phase specifically changes from 10^{-7} to 10^{-8} m [160].

A one-dimensional, steady-state, isothermal agglomerate model was developed by Wang *et al.* [161]. In this model, the cathode catalyst layer is assumed to consist of uniformly distributed spherical agglomerates with radius R_a and void space. The ohmic losses within the solid are ignored, hence the potential within the agglomerate is constant. The diffusion and oxygen reaction within the agglomerate is given as [161]:

$$D_a^{eff} \frac{1}{r^2} \frac{d}{dr}\left(r^2 \frac{dC_{O_2}}{dr} \right) = -\frac{j_c}{nF} \ , \tag{2.48}$$

where D_a^{eff} is the effective diffusivity of oxygen in the porous agglomerate and j_c is the volumetric transfer current. When oxygen concentration in the agglomerate is $C_{O_2}^{s}$, an analytical solution to Eq. (2.48) is given as [161]:

$$C_{O_2} = C_{O_2}^{s} \frac{R_a}{r} \frac{\sinh(\phi r)}{\sinh(\phi R_a)} \ , \tag{2.49}$$

where the product ϕR_a is commonly called the Thiele modulus and is defined as:

$$\phi R_a = \sqrt{\frac{A_{av} i_{0,c}^{ref}}{nFD_a^{eff} C_{O_2}^{ref}}} R_a \exp\left(\frac{\alpha_c F}{2RT} \eta \right). \tag{2.50}$$

The current produced in the agglomerate, I_a, is obtained by using Faraday's law and Eq. (2.49):

$$I_a = nF(4\pi R_a^2)N_{O_2}(r = R_a) = -4\pi nFR_a D_a^{eff} C_{O_2}^s [\phi R_a \coth(\phi R_a) - 1], \tag{2.51}$$

where $N_{O_2}(r = R_a)$ is the oxygen flux at the agglomerate surface, and concentration $C_{O_2}^s$ is related to the gas concentration in the void space, $C_{O_2'g}$, by Henry's law:

$$C_{O_2}^s = H_{O_2} C_{O_2'g} \ , \tag{2.52}$$

where H_{O_2} is Henry's constant for the oxygen gas.

The current density variation in the macroscopic catalyst scale, $i(x)$, may be obtained from the proton mass balance in the layer, based on the solution of the current in the agglomerate, Eq. (2.51). Thus,

$$\frac{di}{dx} = -\rho_a I_a \ , \tag{2.53}$$

where ρ_a is the density of the agglomerates in the catalyst layer and is defined by:

$$\rho_a = \frac{1 - \varepsilon_c}{(4/3)\pi R_a^3} \ , \tag{2.54}$$

where ε_c is the porosity of the catalyst layer. Also, the overpotential is governed by Ohm's law:

$$\frac{d\eta}{dx} = \frac{i}{\kappa^{eff}} \quad . \tag{2.55}$$

The oxygen concentration in the gas pores may be obtained from Eq. (2.53) and Fick's law:

$$nFD_{O_2'c}^{eff} \frac{d^2 C_{O_2'g}}{dx^2} = -\rho_a I_a \quad , \tag{2.56}$$

where $D_{O_2'c}^{eff}$ is the effective oxygen diffusivity in the gas phase. The agglomerate-type models agree better with the physical picture and they are easily implemented in fuel-cell simulation.

CONCLUSION

This part of the thesis provided a background to the basic components of a PEM fuel cell system and their respective functions. General overviews of numerical models of dynamics within PEMFC structures, highlighting governing equations, were also discussed, as well as the applicable theoretical framework employed in the PEM fuel cell modelling carried out in this thesis. The numerical models were implemented in the CFD code employed in this study and the results are reported in Chapters 4 to 6 of this thesis.

3

CHAPTER 3: NUMERICAL MODELLING FRAMEWORK

3.1 INTRODUCTION

In this chapter, we present the numerical and optimisation procedures employed in this research. Numerical modelling provides key benefits to fuel cell designers. It enables the design and building of system components in parallel without other stack hardware being in place. Therefore, as a result of numerical approaches to the design, the production cost of a fuel cell is relatively lower when compared to cost resulting from trial and error design approach, which is often exacerbated by expensive fuel cell hardware components. Hence, the role of numerical modelling in fuel cell production cannot be overemphasised. In this chapter, a general overview is presented of domain discretisation and optimisation techniques employed in fuel cell models used in this study. However, further details regarding grid independence and boundary conditions, as applied for each fuel cell modelling design problem in this thesis, are presented in subsequent sections, i.e., in Chapters 4-6.

3.2 NUMERICAL METHOD

The numerical method involves the flow modelling, discretisation of the flow domain, solving the flow governing equations and data processing. The numerical study was conducted by using the finite volume method [162]. A commercial computational fluid dynamics (CFD) code, ANSYS Fluent® [163] with Gambit® [164] as a pre-processor, is used. The CFD code has an add-on package for fuel cells. The detailed analysis of the numerical modelling techniques will be discussed later, in subsequent sections.

3.2.1 NUMERICAL MODELLING PROCEDURES

The governing sets of mathematical equations that describe the flow field in the modelled fuel cells are based on fundamental fluid dynamics principles, mass conservation, conservation of momentum and conservation of energy. CFD involves the numerical solving of Navier-Stokes and energy equations on a discritised domain. This numerical process commences by first defining the domain and thereafter creating the grid. The grid generation is basically the division of the domain into smaller control volumes. Generally, the numerical algorithm integrates the governing equations over the control volumes and, with the aid of the discretisation, the integral equations are converted into algebraic equations which are then solved iteratively [162]. Navier-Stokes and energy equations are then solved in these smaller volumes. The CFD code employed in this research solves these equations on a discretised domain when relevant flow boundary conditions are specified. The general form of the equation in vector form has been previously presented in section 2.4.1 of this thesis (Eqs. 2.4-2.9).

In modelling the fuel cell, some basic assumptions were made:

- the cell operates under steady-state conditions;
- isothermal boundary conditions were used for external walls;
- the flow in the cell is considered to be laminar;
- reactant and products are assumed to be ideal gas mixtures; and
- the electrode is assumed to be an isotropic and homogeneous porous medium.

These assumptions could be varied when required and additional assumptions may also be specified for a specific fuel cell model as will be shown in Chapters 4-6. The numerical analysis is divided into three stages: pre-processing, the solver (solution technique) and post-processing. The geometry development and grid generation within the flow domain is the pre-processing stage, while solving the flow governing equation at various nodal points within the flow domain is regarded as the solver or

solution technique. The results analysis which involves graphical presentation of simulation data outputs, contour, velocity fields and floods of various parameters are classified as post-processing. A commercial automated grid generator, Gambit® (Geometry and Mesh Building Intelligent Toolkit) that works with a graphical user interface in grid creation, has been used to generate the grid for the pre-processing stage. Gambit® has an added advantage of being able to parameterise the source file of the model domain. This advantage enables a quasi-automation of the grid generation by using journal files which are text files that contain commands that indicate the steps to be followed in the design of the model of interest. The use of the journal files eliminates the need for the graphical user interface or the repetition involved in its usage. ANSYS Fluent® commercial software was used as the solver and part of the post processing. However, the major part of the post-processing was carried out using KaleidaGraph 4.0 software.

Several works have been done towards development of metrics for validation and verification of the computational code used in fluid flow modelling. American Institute of Aeronautics and Astronautics (AIAA) and American Society of Mechanical Engineers (ASME) have also declared policy statements and guidelines for the verification and validation of computational fluid dynamics simulations [43, 44]. These metrics include assessment for iterative convergence, spatial grid convergence and comparison of the CFD results to experimental data. These criteria are used in this thesis for the validation of the solved models. Numerical models used in solving each proposed fuel cell problem in this thesis are first constructed, after which the model is verified by conducting grid independence tests and comparing specific cases against other reported studies in the literature. Modelling validation was done largely by comparison with reported modelling and experimental studies in the literature and this is presented in subsequent sections, i.e., Chapters 4-6. The detail grid adaptation technique for each fuel cell model and the time ranges for each simulation will be presented in subsequent chapters in relation to each model examined. The simulations were carried out on an Intel® Core(TM) 2Duo 3.00 GHz PC with 3.24 GB of DDRam.

3.3 NUMERICAL OPTIMISATION

Recent advancement in digital computer technology has spurred outstanding progress in the area of numerical methods for optimisation. Several methods have been developed for unconstrained and constrained optimisation [165, 166]. Engineering applications for optimisation usually involve solving a nonlinear constrained optimisation problem. Nonlinear constrained problems basically involve the search for a minimum of a nonlinear objective function subject to a set of nonlinear constraints. Numerical optimisation deals with determining the best solution to problems which can be expressed mathematically or numerically. In other words, it implies choosing the best element from a range of available alternatives.

3.3.1 CONSTRAINED OPTIMISATION

Consider the constrained optimisation problem of the general mathematical form:

$$\min f(\mathbf{x}); \mathbf{x} = [x_1, x_2, \ldots\ldots, x_i, \ldots\ldots, x_n]^T, \mathbf{x} \in R^n$$

subject to constraints below:

$$\begin{aligned} &g_j(\mathbf{x}) \leq 0;\ j = 1,2,\ldots\ldots,\ m \\ &h_k(\mathbf{x}) = 0;\ k = 1,2,\ldots\ldots,\ p < n \end{aligned} \tag{3.1}$$

The function $f(\mathbf{x})$ is the objective function to be minimised (or maximised). The $g_j(\mathbf{x})$ and $h_k(\mathbf{x})$ represents the inequality and equality constraint functions, respectively. The components $x_i, i = 2,\ldots\ldots, n$ of $\boldsymbol{x}$ are referred to as the design variables. The optimum vector $\boldsymbol{x}$ that solves the problem denoted by Eq. (3.1) is denoted by the vector:

$$x^* = [x_1^*, x_2^*, ..., x_n^*]^T, \tag{3.2}$$

with the corresponding lowest function value $f(\mathbf{x}^*)$ subject to the given inequality and equality constraints.

There are different approaches to solving the optimisation problem described in Eq. 3.1. An approach is to use the gradient-based algorithms [166] (i.e., successive approximation sequential quadratic programming (SQP) method), or stochastic methods (genetic algorithm). The use of genetic algorithm methods is usually too expensive in terms of number of function evaluations (numerical simulations) when compared with SQP [167, 168]. In this thesis, a relatively new gradient-based and successive approximation Dynamic-Q method of Snyman and Hay [169] is employed. This method has been found to be of equal competitiveness to the conventional SQP method [169], with an advantage of being able to handle problems with severe noise and mixed integer problems [170, 171]. The Dynamic-Q method consists of applying the dynamic trajectory, LFOPC (Leapfrog Optimisation Program for Constrained Problems) optimisation algorithm, to successive quadratic approximations of the actual optimisation problem [169]. The Dynamic-Q method is capable of handling general constrained optimisation problems, and it is discussed in detail in the subsequent section.

3.3.2 THE DYNAMIC-Q METHOD

The Dynamic-Q algorithm method [172] employed in this study uses the LFOP algorithm [173, 174] to handle constrained problems and which includes the use of penalty function approach that is implemented in three distinct phases to increase the capability of obtaining optimal design in a short span of time. Considering a general optimisation problem depicted in Eq. (3.1), the associated penalty function that

transforms the constrained problem to an unconstrained problem form, is thus formulated as [173]:

$$p(\boldsymbol{x}) = f(\boldsymbol{x}) + \sum_{j=1}^{m} \rho_j g_j^2(\boldsymbol{x}) + \sum_{j=1}^{p} \beta_k h_k^2(\boldsymbol{x}), \tag{3.3}$$

where $\rho_j = \begin{cases} 0 \; if g_j(\boldsymbol{x}) \leq 0 \\ \alpha_j \; if g_j(\boldsymbol{x}) > 0 \end{cases}$.

To increase the simplicity of the algorithm, the penalty parameters α_j and β_k takes the same large positive value of μ and the higher the value of μ, the more accurate the obtained solution. Meanwhile, at extreme values of μ, the optimisation problem becomes ill-conditioned. This is resolved by increasing the penalty function piece-wise until a favourable limit value of μ is obtained and then keeping it constant at this limit value until convergence is achieved [175]. The LFOP dynamic trajectory method phases applied to the penalty function are highlighted below.

Phase 0:

Given an initial starting guess of the design variables $\mathbf{x}^0$, the LFOP is applied with some overall penalty parameter μ_0 to $P(\mathbf{x}, \mu_0)$. This gives an optimum design variable vector $\mathbf{x}^*(\mu_0)$ at convergence. The constraints are checked at this optimum value to ensure that no active constraints are neglected (violated). If none of the active constraints are violated, the optimal point is taken as the actual optimal minimum of the optimisation problem being solved and the algorithm is subsequently terminated.

Phase 1:

In a case where there is an active constraint being violated after checks in Phase 0, this phase is initialised. The initialisation process involves applying LFOP with an increasing value of μ and using the obtained optimum ($\mathbf{x}^*(\mu_0)$) in phase 0 as the initial guess. Thereafter, the penalty parameter is then minimised and active constraints are identified. If no active constraints are violated, the optimisation algorithm is terminated and the obtained solution $\mathbf{x}^*(\mu_1)$ is accepted as the optimal solution of the optimisation problem.

Phase 2:

This phase uses the optimal solution from the preceding Phase 1 as the starting guess to apply the LFOP. The algorithm will search for the optimal solution which corresponds to the intersection of the active constraints. During the search, if the active constraints do not intersect, the algorithm will find the best probable solution, which is usually close enough to the actual solution with the lowest possible constraint violation.

3.3.3 DYNAMIC-Q APPROACH: CONSTRUCTING SPHERICAL QUADRATIC SUBPROBLEMS

Dynamic-Q offers a robust optimisation algorithm due to its capability to deal with numerical analyses from CFD and finite element method (FEM) simulations. It does this by handling associated noises generated due to errors created by environmental influences, grid changes, incomplete convergence and numerical accuracy of the computer. The numerical computational time (for an objective function not analytically given or expensive to compute numerically) is reduced in the Dynamic-Q approach by substituting computationally expensive functions by simpler spherically quadratic approximate functions obtained from a few expensive function evaluations (simulations). These approximate functions are utilised to construct successive sub-

problems $P[i], i = 0,1,2,....$ at successive design iteration points i^k. The approximated function can be an objective function and/or the constraint function depending on the optimisation problem being handled. In this Dynamic-Q algorithm, the classical steepest descent (SD) algorithm method used to solve the general function of the form $f(x)$ is modified for better overall performance by applying the SD method successfully to a sequence of very simple quadratic approximations of $f(x)$. The identical curvature entries along the diagonal of the Hessian, means that the level surfaces of the quadratic approximation $\tilde{f}_k(x)$, are concentric hyper-spheres. Hence, the modified classical steepest descent algorithm is aptly referred to as spherical quadratic approximations. The constructions of these spherical quadratic approximations are described below [175, 176]:

$$\begin{aligned}
\tilde{f}(\mathbf{x}) &= f(\mathbf{x}^i) + \nabla^T f(\mathbf{x}^i)(\mathbf{x}-\mathbf{x}^i) + \frac{1}{2}(\mathbf{x}-\mathbf{x}^i)^T \mathbf{A}(\mathbf{x}-\mathbf{x}^i) \\
\tilde{g}_j(\mathbf{x}) &= g_j(\mathbf{x}^i) + \nabla^T g_j(\mathbf{x}^i)(\mathbf{x}-\mathbf{x}^i) + \frac{1}{2}(\mathbf{x}-\mathbf{x}^i)^T \mathbf{B}_j(\mathbf{x}-\mathbf{x}^i) \\
\tilde{h}_k(\mathbf{x}) &= h_k(\mathbf{x}^i) + \nabla^T h_k(\mathbf{x}^i)(\mathbf{x}-\mathbf{x}^i) + \frac{1}{2}(\mathbf{x}-\mathbf{x}^i)^T \mathbf{C}_k(\mathbf{x}-\mathbf{x}^i)
\end{aligned} \tag{3.4}$$

$\mathbf{A}$, $\mathbf{B}_j$ and $\mathbf{C}_k$ are Hessian matrices of the objective, inequality and equality functions, respectively, and often take on the simple forms:

$$\begin{aligned}
\mathbf{A} &= \operatorname{diag}(a, a, ..., a) = a\,\mathbf{I} \\
\mathbf{B}_j &= b_j\,\mathbf{I} \\
\mathbf{C}_k &= c_k\,\mathbf{I} \quad ,
\end{aligned} \tag{3.5}$$

where **I** represents the identity matrix.

∇^T, $\nabla^T g_j$ and $\nabla^T h_k$ are gradient vectors. If these vectors are not known analytically, they are approximated from functional data by means of first-order forward finite differences [176].

Intermediate move limits are employed in the Dynamic-Q algorithm to achieve convergence in a controlled and stable form. The move limit δ_j takes on the form of a constraint by limiting the movement of each design variable, $\mathbf{x}_j^{(i-1)}$, by preventing the new design point from moving too far away from the current design point. An additional constraint of the form is:

$$\begin{aligned} \mathbf{x}_j - \mathbf{x}_j^{(i-1)} - \delta_j &\leq 0 \\ -\mathbf{x}_j^{(i-1)} + \mathbf{x}_j - \delta_j &\leq 0 \end{aligned} \quad ; j = 1, 2, \ldots, n \quad . \tag{3.6}$$

The Dynamic-Q algorithm terminates when the following step size and function value criteria are satisfied:

- <u>Step size:</u>

$$\Delta x_{norm} = \frac{\| x^k - x^{k-1} \|}{1 + \| x^k \|} < \varepsilon_x \ ; \tag{3.7}$$

- <u>Function value:</u>

$$\Delta f_{norm} = \frac{| f^k - f_{best} |}{1 + | f_{best} |} < \varepsilon_f \ ; \tag{3.8}$$

where ε_x and ε_f are the step sizes and function value tolerances, respectively.

3.3.4 THE OBJECTIVE AND CONSTRAINT FUNCTIONS GRADIENT APPROXIMATION

The Snyman Dynamic-Q method requires the gradients of the objective and constraint functions. When these gradient functions are not analytically available, the components of the gradients are calculated as follows:

$$\frac{\partial f(\mathbf{x})}{\partial x_i} = \frac{f(\mathbf{x}+\Delta\mathbf{x}_i) - f(\mathbf{x})}{\Delta x_i}, \quad i = 1,2,...,n \quad , \tag{3.9}$$

where the differencing step size is given as:

$$\Delta\mathbf{x}_i = [0,0,...,\Delta x_i,...,0]^T \quad . \tag{3.10}$$

The gradients of the inequality and equality constraint function components used in the spherical approximation are similarly approximated and depicted in the Eq. (3.10). Thus,

$$\begin{aligned} \frac{\partial g_i(\mathbf{x})}{\partial x_i} &= \frac{g_i(\mathbf{x}+\Delta\mathbf{x}_i) - g_i(\mathbf{x})}{\Delta x_i}, \quad i = 1,2,...,n \quad , \\ \frac{\partial h_i(\mathbf{x})}{\partial x_i} &= \frac{h_i(\mathbf{x}+\Delta\mathbf{x}_i) - h_i(\mathbf{x})}{\Delta x_i}, \quad i = 1,2,...,p \quad , \end{aligned} \tag{3.11}$$

also with the differencing step size being:

$$\Delta\mathbf{x}_i = [0,0,...,\Delta x_i,...,0]^T \quad . \tag{3.12}$$

In practice, new CFD simulation is required to approximate each of the components (i.e., at each optimisation iteration, n+1). This tends to increase the computational

cost but could be reduced by assuming a constant differencing step size for each design variable.

Simulation processes are always accompanied by noises that are introduced by the step size $\Delta\mathbf{x}$, used in the differencing scheme. Therefore, choosing an appropriate step size that gives good results and at the same time eliminates noise generation during simulation, remains very pertinent. This is done by using the Dynamic-Q algorithm. The experience of the modeller to solve this associated problem then comes in handy. To ensure an appropriate step size, different starting guesses should be used a couple of times and, if the converged solution values are the same, then the chosen step size is accepted as sufficient. In cases where the converged solution value differs, the step size should be modified until the variations in the results are eliminated.

In summary, the Dynamic-Q algorithm can be stated as follows [169]:

i. Choose a starting point $\mathbf{x}^1$ and move limits δ_j, $j = 1,2,...,n$ and set $i := 1$.
ii. Evaluate $f(\mathbf{x}^i)$, $g_j(\mathbf{x}^i)$, and $h_k(\mathbf{x}^i)$, as well as $\nabla f(\mathbf{x}^i)$, $\nabla g_j(\mathbf{x}^i)$, and $\nabla h_k(\mathbf{x}^i)$. If termination criteria are satisfied then set $\mathbf{x}^* = \mathbf{x}^i$ and stop.
iii. Construct a local approximation, $P[i]$, to the optimisation problem at $\mathbf{x}^i$, using approximations for the objective and constraint functions.
iv. Solve the approximated sub-problem, $P[i]$, to give $\mathbf{x}^{*i}$, by using LFOPC [173].
v. Set $i := i+1$, $\mathbf{x}^i := \mathbf{x}^{*(i-1)}$ and return to step ii.

3.3.5 ADVANTAGE OF DYNAMIC-Q ALGORITHM

The use of spherically quadratic approximation in the Dynamic-Q algorithm offers a competitive advantage when compared with other methods in terms of the computational and storage requirements. The $O(n^2)$ calculations and storage locations required for the second order derivatives are not required since the second derivatives

of the objective function and constraints are approximated by using function and gradient data. The Dynamic-Q computational and storage resources are thus practically reduced to O(n). At the most, $4 + p + q + r + s \quad n -$ vectors need be stored (where p, q, r and s are the number of inequality and equality constraints and the number of lower and upper limits of the variables, respectively). The storage savings becomes highly significant when the number of variables becomes large [169]. Therefore, the particular strength of the Dynamic-Q method makes it well suited for optimisation of engineering problems with large number of variables.

CONCLUSION

This chapter focused on the description of numerical methods and mathematical optimisation algorithm used in this study. The DYNAMIC-Q, which builds on the LFOPC algorithm, is discussed in detail. The strength of this mathematical optimisation choice was also highlighted in terms of storage savings where large numbers of variables and noise handling during simulation were being considered.